

WEAK SINDY FOR PARTIAL DIFFERENTIAL EQUATIONS

DANIEL A. MESSENGER* AND DAVID M. BORTZ*

Abstract. We extend the WSINDy (Weak SINDy) method of sparse recovery introduced in [20] to the setting of partial differential equations (PDEs). As in the case of ODE discovery, the weak form replaces pointwise approximation of derivatives with local integrations against test functions and achieves effective machine-precision recovery of weights from noise-free data (i.e. below the tolerance of the simulation scheme) as well as natural robustness to noise without the use of noise filtering. The resulting WSINDy-PDE algorithm uses separable test functions implemented efficiently via convolutions for discovery of PDE models with computational complexity $\mathcal{O}(NM)$ from datasets with $M = N^{D+1}$ points, or N points in each of $D+1$ dimensions. We demonstrate on several notoriously challenging PDEs the speed and accuracy with which WSINDy-PDE recovers the correct models from datasets with surprisingly large levels of noise (often with noise levels much greater than 10%).

Key words. data-driven model selection, partial differential equations, sparse recovery, Galerkin method, white noise, Kuramoto-Sivashinsky, nonlinear Schrödinger's, Sine-Gordon, reaction-diffusion, Navier-Stokes.

AMS subject classifications. 65M60,35-04,62-08,62J07

1. Introduction. Stemming from Akaike's seminal work in the 1970's [1, 2], research into the automatic creation of accurate mathematical models from data has progressed dramatically. In the last 20 years, substantial developments have been made at the interface of applied mathematics and statistics to design data-driven model selection algorithms that are both statistically rigorous and computationally efficient (see [4, 17, 18, 31, 38, 39] for both theory and applications). An important achievement in this field was the formulation and subsequent discretization of the system discovery problem in terms of a candidate basis of nonlinear functions evaluated at the given dataset, together with a sparsification measure to avoid overfitting [8]. In [33] the authors extended this framework to the context of catastrophe prediction and used compressed sensing techniques to enforce sparsity. More recently, this approach has been generalized as the SINDy algorithm (Sparse Identification of Nonlinear Dynamics) [5] and successfully used to identify a variety of discrete and continuous dynamical systems.

The wide applicability, computational efficiency, and interpretability of the SINDy algorithm has spurred an explosion of interest in the problem of identifying nonlinear dynamical systems from data [7, 23, 9, 10, 12, 32, 19]. In addition to the sparse regression approach adopted in SINDy, some of the primary techniques include Gaussian process regression [25], deep neural networks [27, 34, 17], Bayesian inference [44, 45, 37] and classical methods from numerical analysis [13, 15, 40]. The variety of approaches for model discovery from data qualitatively differ in the interpretability of the resulting data-driven dynamical system, the practicality of the algorithm, and the robustness to noise, scale separation, etc. For instance, a neural-network based data-driven dynamical system does not easily lend itself to physical interpretation. As well, certain sparsification techniques are not practical to the general scientific community where the problem of system identification from data is ubiquitous, either due to difficulty in arriving at optimal hyperparameters or lack of computational efficiency. The SINDy algorithm allows for direct interpretations of the dynamics

*Department of Applied Mathematics, University of Colorado, Boulder, CO 80309-0526, USA.
(daniel.messenger@colorado.edu, dmbortz@colorado.edu).

from identified differential equations and uses sequentially thresholded least-squares to enforce sparsity, which has its setbacks (see the discussion surrounding equation (3.16)) but can be implemented efficiently and has been proven to converge to sparse local minimizers in a bounded number of iterations [43].

The aim of the present article is to extend the WSINDy method (Weak SINDy) for recovering ordinary differential equations (ODEs) from data to the context of partial differential equations (PDEs) [20]. WSINDy is a Galerkin-based data-driven model selection algorithm that utilizes the weak form of the dynamics in a sparse regression framework. By integrating in time against compactly-supported test functions, WSINDy avoids approximation of pointwise derivatives which are known to result in low robustness to noise [26]. In [20] it is shown that by integrating against a suitable choice of test functions, correct ODE model terms can be identified with machine-precision recovery of weights (i.e. below the tolerance of the data simulation scheme) from noise-free synthetic data, and for data sets with large noise, WSINDy successfully recovers the correct model terms without noise filtering. For PDE identification, as we will show here, this trend still holds, and appears to be amplified: WSINDy_PDE recovers PDE models with high accuracy from low-noise data and can handle a surprising amount of noise, with noise levels (defined in (4.1)) as high as 50% (see Table 3). In addition, WSINDy_PDE enjoys a fast implementation achieved by rewriting the proposed weak dynamics in the form of convolutions with test functions that are separable over the given coordinates. For measurement data with N points in each of the $D + 1$ space-time dimensions ($M = N^{D+1}$ total data points), the resulting algorithmic complexity of WSINDy_PDE is at worst $\mathcal{O}(NM)$, with constant depending on the size of the candidate model library. With subsampling the cost is further reduced.

Learning PDEs from data is a relatively recent endeavor, due in large part to previous computational burdens, and much progress has been made in the last several years. Extension of SINDy to PDEs was achieved in [26], where machine learning was used to arrive at appropriate hyperparameters. Many other predominant approaches for learning dynamical systems (Gaussian processes, deep learning, Bayesian inference, etc) have since been extended to the discovery of PDEs [6, 21, 16, 17, 36, 35, 42, 41, 30, 38]. The vast majority of PDE discovery methods rely on pointwise derivative approximations, prior noise filtering and/or black-box routines (e.g. neural networks). WSINDy_PDE falls into a class of methods for discovering PDEs in a non-differential form. The use of integral equations for system identification was proposed as early as the 1980's [8] and was carried out in [28] in the context of ODEs using compressed sensing techniques to enforce sparsity. More recently, the authors of [24] and [41] combine neural network-based recovery schemes with integral and abstract evolution equations to recover PDE dynamics.

To the best of our knowledge, WSINDy_PDE is the first PDE discovery method that does not require any pointwise derivative approximations, black-box routines or data denoising. A similar approach to WSINDy_PDE, dubbed Variational System Identification (VSI), was developed in [35], where classical finite element discretizations were utilized in the identification of reaction-diffusion systems. VSI uses backward Euler for time differentiation and requires datapoints to be given at the nodes of a finite element basis in order to take spatial derivatives of the dataset using the underlying basis. In contrast, WSINDy_PDE avoids approximation of derivatives entirely by integrating by parts in both space and time against smooth compactly-supported test functions, enabling WSINDy_PDE to recover PDEs from datasets with much higher noise levels. In addition, by removing the requirement that the PDE be reformulated in a symmetric

variational form, WSINDy-PDE allows for identification of much more general PDE systems. Conversely, by explicitly accounting for boundary terms, VSI allows for the identification of boundary conditions, which is something WSINDy-PDE is not currently designed to discover.

The outline of the article is as follows. In Section 2 we introduce the system discovery problem and notation to be used throughout. We introduce WSINDy-PDE (Algorithm 3.2) in Section 3 along with several computational subtleties that enable rapid and accurate system identification. Section 4 contains numerical model discovery results for a range of nonlinear PDEs, including several vast improvements on existing results in the literature. We conclude the exposition in Section 5 with natural next directions for this line of research and a brief comparison between WSINDy-PDE and other existing system discovery methods.

2. Problem Statement and Notation. Let \mathbf{U} be a spatiotemporal dataset given on the spatial grid $\mathbf{X} \subset \overline{\Omega}$ over timepoints $\mathbf{t} \subset [0, T]$ where Ω is an open, bounded subset in \mathbb{R}^D , $D \geq 1$. In the cases we consider here, Ω is rectangular and the spatial grid is given by a tensor product of one-dimensional grids $\mathbf{X} = \mathbf{X}_1 \otimes \cdots \otimes \mathbf{X}_D$, where each $\mathbf{X}_d \in \mathbb{R}^{N_d}$ for $1 \leq d \leq D$ has equal spacing Δx , and the time grid $\mathbf{t} \in \mathbb{R}^{N_{D+1}}$ has equal spacing Δt . The dataset \mathbf{U} is then a $(D+1)$ -dimensional array with dimensions $N_1 \times \cdots \times N_{D+1}$. We write $h(\mathbf{X}, \mathbf{t})$ to denote the $(D+1)$ -dimensional array obtained by evaluating the function $h : \mathbb{R}^D \times \mathbb{R} \rightarrow \mathbb{C}$ at each of the points in the computational grid (\mathbf{X}, \mathbf{t}) . Individual points in (\mathbf{X}, \mathbf{t}) will often be denoted by $(\mathbf{x}_k, t_k) \in (\mathbf{X}, \mathbf{t})$ where

$$(\mathbf{x}_k, t_k) = (\mathbf{X}_{k_1, \dots, k_D}, t_{k_{D+1}}) = (x_{k_1}, \dots, x_{k_D}, t_{k_{D+1}}) \in \mathbb{R}^D \times \mathbb{R}.$$

In a mild abuse of notation, for a collection of points $\{(\mathbf{x}_k, t_k)\}_{k \in [K]} \subset (\mathbf{X}, \mathbf{t})$, the index k plays a double role as a single index in the range $[K] := \{1, \dots, K\}$ referencing the point $(\mathbf{x}_k, t_k) \in \{(\mathbf{x}_k, t_k)\}_{k \in [K]}$ and as a multi-index on $(\mathbf{x}_k, t_k) = (\mathbf{X}_{k_1, \dots, k_D}, t_{k_{D+1}})$. This is particularly useful for defining a matrix $\mathbf{G} \in \mathbb{C}^{K \times J}$ of the form

$$\mathbf{G}_{k,j} = h_j(\mathbf{x}_k, t_k)$$

(as in equation (3.6) below) where $(h_j)_{j \in [J]}$ is a collection of J functions $h_j : \mathbb{R}^D \times \mathbb{R} \rightarrow \mathbb{C}$ evaluated at the set of K points $\{(\mathbf{x}_k, t_k)\}_{k \in [K]} \subset (\mathbf{X}, \mathbf{t})$.

We assume that $\mathbf{U} = u(\mathbf{X}, \mathbf{t}) + \epsilon$ for i.i.d noise ϵ where u satisfies the PDE

$$(2.1) \quad D^{\alpha^0} u(x, t) = D^{\alpha^1} g_1(u(x, t)) + D^{\alpha^2} g_2(u(x, t)) + \cdots + D^{\alpha^S} g_S(u(x, t)), \quad x \in \Omega, t \in (0, T).$$

The problem we aim to solve is the identification of functions $(g_s)_{s \in [S]}$ and corresponding partial derivatives $(D^{\alpha^s})_{s \in [S]}$ that govern the evolution of u according to $D^{\alpha^0} u$, given the dataset \mathbf{U} and computational grid (\mathbf{X}, \mathbf{t}) . Here and throughout we use the multi-index notation $\alpha^s = (\alpha_1^s, \dots, \alpha_D^s, \alpha_{D+1}^s) \in \mathbb{N}^{D+1}$ to denote partial derivation with respect to $x = (x_1, \dots, x_D)$ and t , so that

$$D^{\alpha^s} u(x, t) = \frac{\partial^{\alpha_1^s + \cdots + \alpha_D^s + \alpha_{D+1}^s}}{\partial x_1^{\alpha_1^s} \cdots \partial x_D^{\alpha_D^s} \partial t^{\alpha_{D+1}^s}} u(x, t).$$

In particular, in this paper we demonstrate our method of system identification on the following PDEs in

one and two spatial dimensions:

$$\begin{aligned}
\text{(Kuramoto-Sivashinsky)} \quad & u_t = -\frac{1}{2}(u^2)_x - u_{xx} - u_{xxxx} \\
\text{(Nonlinear Schrödinger)} \quad & u_t = -\frac{i}{2}u_{xx} + |u|^2u, \\
\text{(Sine Gordon)} \quad & u_{tt} = \Delta u - \sin(u) \\
\text{(Reaction-Diffusion)} \quad & \begin{cases} u_t = \nu_u \Delta u + \lambda(A)u - \omega(A)v \\ v_t = \nu_v \Delta v - \omega(A)u + \lambda(A)v \end{cases} \\
\text{(Navier-Stokes)} \quad & \begin{cases} \omega_t = -\nabla \cdot (\boldsymbol{\omega} \mathbf{u}^T) + \frac{1}{Re} \Delta \boldsymbol{\omega} \\ \boldsymbol{\omega} = \nabla \times \mathbf{u}. \end{cases}
\end{aligned}$$

Note that for incompressible fluids, the conservative flux term in the Navier-Stokes equations satisfies

$$\nabla \cdot (\boldsymbol{\omega} \mathbf{u}^T) = (\nabla \cdot \mathbf{u})\boldsymbol{\omega} + (\mathbf{u} \cdot \nabla)\boldsymbol{\omega} = (\mathbf{u} \cdot \nabla)\boldsymbol{\omega}.$$

A compelling feature of WSINDy_PDE is that the conservative form of the Navier-Stokes equations is discovered regardless of the compressibility constraint (see Section 4.5 for a more involved discussion).

3. Weak Formulation and Discretization. To arrive at a computationally tractable model recovery problem, we assume that the set of multi-indices $(\alpha^s)_{s \in [S]}$ together with α^0 contains the set of true partial derivatives that govern the evolution of u and that $(g_s)_{s \in [S]} \subset \text{span}(f_j)_{j \in [J]}$ where the family of functions $(f_j)_{j \in [J]}$ (referred to as the trial functions) is known beforehand. This enables us to rewrite (2.1) as

$$(3.1) \quad D^{\alpha^0} u = \sum_{s=1}^S \sum_{j=1}^J \mathbf{w}_{(s-1)J+j}^* D^{\alpha^s} f_j(u),$$

so that discovery of the correct PDE is reduced to a finite-dimensional problem of recovering the weight vector $\mathbf{w}^* \in \mathbb{R}^{SJ}$, which is assumed to be sparse.

To convert the PDE into its weak form, we multiply equation (3.1) by a smooth test function $\psi(x, t)$, compactly-supported in $\Omega \times (0, T)$, and integrate over the spacetime domain,

$$\langle \psi, D^{\alpha^0} u \rangle = \sum_{s=1}^S \sum_{j=1}^J \mathbf{w}_{(s-1)J+j}^* \langle \psi, D^{\alpha^s} f_j(u) \rangle,$$

where the L^2 -inner product is defined $\langle \psi, f \rangle := \int_0^T \int_{\Omega} \psi^*(x, t) f(x, t) dx dt$ and ψ^* denotes the complex conjugate of ψ , although in what follows we integrate against only real-valued test functions and will omit the complex conjugation. Using the compact support of ψ and Fubini's theorem, we then integrate by parts as many times as necessary to arrive at the following weak form of the dynamics:

$$(3.2) \quad \langle (-1)^{|\alpha^0|} D^{\alpha^0} \psi, u \rangle = \sum_{s=1}^S \sum_{j=1}^J \mathbf{w}_{(s-1)J+j}^* \langle (-1)^{|\alpha^s|} D^{\alpha^s} \psi, f_j(u) \rangle,$$

where $|\alpha^s| := \sum_{d=1}^{D+1} \alpha_d^s$ is the order of the multi-index. For example, with $D^{\alpha^s} = \frac{\partial^{2+1}}{\partial x^2 \partial y}$, integration by parts occurs twice with respect to the x -coordinate and once with respect to y , so that $|\alpha^s| = 3$ and $(-1)^{|\alpha^s|} = -1$.

Using an ensemble of test functions $(\psi_k)_{k \in [K]}$, we then discretize the integrals in (3.2) with $f_j(u)$ replaced by $f_j(\mathbf{U})$ (i.e. evaluated at the observed data \mathbf{U}) to arrive at the linear system

$$\mathbf{b} = \mathbf{G}\mathbf{w}^*$$

defined by

$$(3.3) \quad \begin{cases} \mathbf{b}_k = \left\langle (-1)^{|\alpha^0|} D^{\alpha^0} \psi_k, \mathbf{U} \right\rangle, \\ \mathbf{G}_{k,(s-1)J+j} = \left\langle (-1)^{|\alpha^s|} D^{\alpha^s} \psi_k, f_j(\mathbf{U}) \right\rangle, \end{cases}$$

where $\mathbf{b} \in \mathbb{R}^K$, $\mathbf{G} \in \mathbb{R}^{K \times SJ}$ and $\mathbf{w}^* \in \mathbb{R}^{SJ}$. By some abuse of notation, the inner products appearing in (3.3) are numerical approximations that depend on the quadrature rule chosen by the user (specified in Section 3.1), whereas the inner products in (3.2) are continuous and exact. In this way, solving $\mathbf{b} = \mathbf{G}\mathbf{w}^*$ for the weights \mathbf{w}^* allows for the recovery of the differential model (3.1) without the need to numerically approximate derivatives, this operation having been entirely replaced by integration against test functions.

The Gram matrix $\mathbf{G} \in \mathbb{R}^{K \times SJ}$ and right-hand side $\mathbf{b} \in \mathbb{R}^K$ defined in (3.3) conveniently take the same form regardless of the spatial dimension D , as their dimensions only depend on the number of test functions K and the size $(S+1)J$ of the model library, composed of J trial functions and $S+1$ candidate differential operators, given by the multi-indices $\boldsymbol{\alpha} := (\alpha^s)_{0 \leq s \leq S}$. To formulate the WSINDy_PDE algorithm for constructing and solving $\mathbf{b} = \mathbf{G}\mathbf{w}^*$, we must therefore choose the set of test functions $(\psi_k)_{k \in [K]}$, the set of trial functions $(f_j)_{j \in [J]}$, the set of multi-indices $\boldsymbol{\alpha} := (\alpha^s)_{0 \leq s \leq S}$, the quadrature rule for discretizing integrals, and the method of enforcing sparsity in the weight vector \mathbf{w}^* . Below we introduce a convolution-based approach for fast computation of \mathbf{G} and \mathbf{b} that operates efficiently over multi-dimensional arrays by exploiting separability in the test functions. We then discuss the selection of suitable piecewise polynomial test functions designed to yield high accuracy quadrature via the trapezoidal rule, extending the theory from [20]. Pseudocode for the WSINDy_PDE algorithm is given in 3.2, with sparsity enforced using sequentially-thresholded least squares as in the standard SINDy algorithm [5] along with Tikhonoff regularization for poorly-conditioned linear systems.

3.1. Implementation via Convolution. We now restrict to the case of each test function ψ_k being a translation of a reference test function ψ , i.e. $\psi_k(x, t) = \psi(\mathbf{x}_k - x, t_k - t)$ for some collection of points $\{(\mathbf{x}_k, t_k)\}_{k \in [K]} \subset (\mathbf{X}, \mathbf{t})$ (referred to as the query points). The weak form of the dynamics (3.2) over the test function basis $(\psi_k)_{k \in [K]}$ can then be written as a convolution:

$$(3.4) \quad \left(D^{\alpha^0} \psi \right) * u(\mathbf{x}_k, t_k) = \sum_{s=1}^S \sum_{j=1}^J \mathbf{w}_{nJ+j}^* \left(D^{\alpha^s} \psi \right) * f_j(u)(\mathbf{x}_k, t_k).$$

The sign factor $(-1)^{|\alpha^s|}$ appearing in (3.2) after integrating by parts is eliminated in (3.4) due to the sign convention in the integrand of the space-time convolution, which is defined by

$$\psi * u(x, t) := \int_0^T \int_{\Omega} \psi(x - y, t - s) u(y, s) dy ds = \langle \psi(x - \cdot, t - \cdot), u \rangle.$$

Construction of the linear system $\mathbf{b} = \mathbf{G}\mathbf{w}^*$ as a discretization of the convolution form (3.4) over the query points $\{(\mathbf{x}_k, t_k)\}_{k \in [K]}$ can then be carried out efficiently, as we will now demonstrate.

For notational purposes, it is necessary to specify a computational grid $(\mathbf{Y}, \boldsymbol{\tau}) \subset \mathbb{R}^D \times \mathbb{R}$ for the reference test function ψ . Let the support of ψ be contained within the spacetime domain

$$\Omega_R := [-b_1, b_1] \times \cdots \times [-b_D, b_D] \times [-b_{D+1}, b_{D+1}] \subset \mathbb{R}^D \times \mathbb{R}$$

where $b_d = m_d \Delta x$ for $d \in [D]$ and $b_{D+1} = m_{D+1} \Delta t$. The domain Ω_R is then completely defined by the integers $\mathbf{m} = (m_d)_{d \in [D+1]}$ which are specified by the user upon selecting a reference test function ψ . The computational grid $(\mathbf{Y}, \boldsymbol{\tau}) \subset \Omega_R$ for ψ is then given by $\mathbf{Y} = \mathbf{Y}_1 \otimes \cdots \otimes \mathbf{Y}_D$ for $\mathbf{Y}_d = (n \Delta x)_{-m_d \leq n \leq m_d}$, $1 \leq d \leq D$, and $\boldsymbol{\tau} = (n \Delta t)_{-m_{D+1} \leq n \leq m_{D+1}}$. Similar to (\mathbf{X}, \mathbf{t}) , we let points $(\mathbf{y}_k, \tau_k) \in (\mathbf{Y}, \boldsymbol{\tau})$ take the form

$$(\mathbf{y}_k, \tau_k) = (\mathbf{Y}_{k_1, \dots, k_D}, \boldsymbol{\tau}_{k_{D+1}})$$

where each index k_d for $d \in [D+1]$ takes values in the range $\{-m_d, \dots, 0, \dots, m_d\}$.

To summarize, the $(D+1)$ -dimensional array $(\mathbf{Y}, \boldsymbol{\tau}) \subset \mathbb{R}^D \times \mathbb{R}$ discretizes the support of ψ at the same spatiotemporal resolution as the dataset \mathbf{U} defined on (\mathbf{X}, \mathbf{t}) . Along each dimension $d \in [D]$, \mathbf{Y} contains $2m_d + 1$ points with spacing Δx , and $\boldsymbol{\tau}$ contains $2m_{D+1} + 1$ points with equal spacing Δt . Finally, where defined, the two grids (\mathbf{X}, \mathbf{t}) and $(\mathbf{Y}, \boldsymbol{\tau})$ are related by

$$(3.5) \quad (\mathbf{x}_k - \mathbf{x}_j, t_k - t_j) = (\mathbf{y}_{k-j}, \tau_{k-j}).$$

We may now rewrite the entries of the linear system $\mathbf{b} = \mathbf{G}\mathbf{w}^*$ as

$$(3.6) \quad \begin{cases} \mathbf{b}_k = \Psi^0 * \mathbf{U}(\mathbf{x}_k, t_k), \\ \mathbf{G}_{k, (s-1)J+j} = \Psi^s * f_j(\mathbf{U})(\mathbf{x}_k, t_k), \end{cases}$$

where $\Psi^s := D^{\alpha^s} \psi(\mathbf{Y}, \boldsymbol{\tau}) \Delta x^D \Delta t$ so that

$$\Psi^s * f_j(\mathbf{U})(\mathbf{x}_k, t_k) \approx \int_0^T \int_{\Omega} D^{\alpha^s} \psi(\mathbf{x}_k - x, t_k - t) f_j(u(x, t)) dx dt.$$

More explicitly, at a given query point $(\mathbf{x}_k, t_k) = (\mathbf{X}_{k_1, \dots, k_D}, t_{k_{D+1}}) \in (\mathbf{X}, \mathbf{t})$, we define the discrete $(D+1)$ -dimensional convolution by

$$\Psi^s * \mathbf{U}(\mathbf{x}_k, t_k) := \sum_{j_1=1}^{N_1} \cdots \sum_{j_{D+1}=1}^{N_{D+1}} \Psi_{k_1-j_1, \dots, k_{D+1}-j_{D+1}}^s \cdot \mathbf{U}_{j_1, \dots, j_{D+1}},$$

which, substituting the definition of Ψ^s ,

$$(3.7) \quad := \sum_{j_1=1}^{N_1} \cdots \sum_{j_{D+1}=1}^{N_{D+1}} D^{\alpha^s} \psi(\mathbf{Y}_{k_1-j_1, \dots, k_{D+1}-j_{D+1}}, \tau_{k_{D+1}-j_{D+1}}) \cdot \mathbf{U}_{j_1, \dots, j_{D+1}} \cdot \Delta x^D \Delta t$$

truncating indices appropriately and using (3.5),

$$(3.8) \quad = \sum_{j_1=k_1-m_1}^{k_1+m_1} \cdots \sum_{j_{D+1}=k_{D+1}-m_{D+1}}^{k_{D+1}+m_{D+1}} D^{\alpha^s} \psi(\mathbf{Y}_{k_1-j_1, \dots, k_D-j_D}, \tau_{k_{D+1}-j_{D+1}}) \cdot \mathbf{U}_{j_1, \dots, j_{D+1}} \cdot \Delta x^D \Delta t$$

$$(3.9) \quad = \sum_{j_1=k_1-m_1}^{k_1+m_1} \cdots \sum_{j_{D+1}=k_{D+1}-m_{D+1}}^{k_{D+1}+m_{D+1}} D^{\alpha^s} \psi(\mathbf{x}_k - \mathbf{x}_j, t_k - t_j) \cdot \mathbf{U}_{j_1, \dots, j_{D+1}} \cdot \Delta x^D \Delta t$$

$$(3.10) \quad \approx \int_0^T \int_{\Omega} D^{\alpha^s} \psi(\mathbf{x}_k - x, t_k - t) u(x, t) dx dt.$$

The factor $\Delta x^D \Delta t$ indicates the use of the trapezoidal rule for numerical integration, which we use throughout as it has been shown to yield nearly negligible quadrature error on the test functions employed in WSINDy-PDE (see Section 3.3 and [20]).

Remark 3.1. As it is written above, for certain k , the summation indices $(j_d)_{d \in [D+1]}$ in the discrete convolution (3.8) may become negative and hence reference invalid entries $\mathbf{U}_{j_1, \dots, j_{D+1}}$ of the dataset \mathbf{U} . One option is to simply set the corresponding summands to zero, however, this violates the compact support arguments that are used to arrive at the weak formulation of the dynamics (3.2). To prevent this, we require the query points $\{(\mathbf{x}_k, t_k)\}_{k \in [K]}$ to satisfy

$$(3.11) \quad m_d + 1 \leq k_d \leq N_d - m_d, \quad d \in [D+1], \quad k \in [K].$$

This corresponds to ensuring that $\psi(\mathbf{x}_k - \cdot, t_k - \cdot)$ is compactly support in $\Omega \times [0, T]$ for each $k \in [K]$ ¹. Recall that compact support of $(\psi_k)_{k \in [K]}$ is required in the weak formulation (3.2). In addition, this implies the restriction $m_d < \frac{N_d-1}{2}$ for each $d \in [D+1]$.

Altogether, the entries of the Gram matrix \mathbf{G} are given in convolution form by

$$\begin{aligned} \mathbf{G}_{k, (s-1)J+j} &= \Psi^s * f_j(\mathbf{U})(\mathbf{x}_k, t_k) \\ &= \sum_{j_1=k_1-m_1}^{k_1+m_1} \cdots \sum_{j_{D+1}=k_{D+1}-m_{D+1}}^{k_{D+1}+m_{D+1}} \Psi_{k_1-j_1, \dots, k_{D+1}-j_{D+1}}^s \cdot f_j(\mathbf{U}_{j_1, \dots, j_{D+1}}) \\ &\approx \int_0^T \int_{\Omega} D^{\alpha^s} \psi(\mathbf{x}_k - x, t_k - t) f_j(u(x, t)) dx dt, \end{aligned}$$

where the query points $\{(\mathbf{x}_k, t_k)\}_{k \in [K]}$ must each satisfy (3.11) and the arrays $\Psi^s := D^{\alpha^s} \psi(\mathbf{Y}, \tau) \Delta x^D \Delta t$ are computed analytically from the user-specified reference test function ψ , including the values $(m_d)_{d \in [D+1]}$ used to determine (\mathbf{Y}, τ) . (Entries of the right-hand side vector \mathbf{b} are similarly defined.) Finally, we now discuss choices made in WSINDy-PDE that allow for efficient and accurate implementation.

3.2. Separable Test Functions. Convolutions in the linear system (3.6) may be computed rapidly if the reference test function ψ is separable over the given coordinates, i.e.

$$\psi(x, t) = \phi_1(x_1) \cdots \phi_D(x_D) \phi_{D+1}(t)$$

¹In MATLAB's implementation of `conv` this is achieved by using the `valid` option.

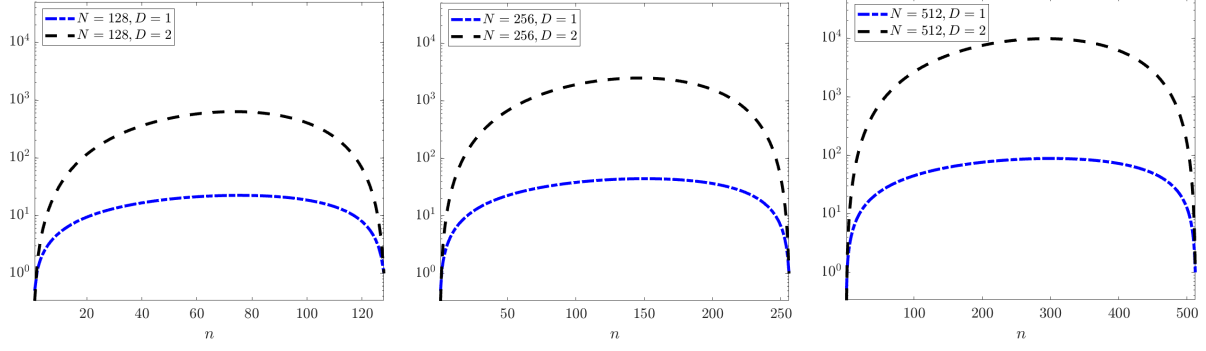


FIG. 3.1. Plots showing reduction in computational cost for separable multi-dimensional convolution $\Psi * \mathbf{U}$ when Ψ and \mathbf{U} have n and N points, respectively, in each $D + 1$ dimensions. For left to right: $N = 128, 256, 512$. Each plot shows the cases $D + 1 = 2$ and $D + 1 = 3$ space-time dimensions. The y-axis shows $C_{\text{naive}}/C_{\text{sep}}$ (equations (3.12) and (3.13)), in other words the factor by which the separable convolution reduces the cost of the naive convolution, versus $n \in [N]$. The right plot shows that when the data \mathbf{U} has $N = 512$ points in each of $D + 1 = 3$ space-time dimensions and ψ is supported on $n = 293$ points in each dimension, then the separable convolution reduces computation time by four orders of magnitude. In general, the reduction in cost increases with N and D .

for one-dimensional functions $(\phi_d)_{d \in [D+1]}$. To demonstrate the reduction in computation costs, if $N_d = N$ for all $1 \leq d \leq D + 1$ and ψ is supported on $n \leq N$ points in each direction of the computational grid $(\mathbf{Y}, \boldsymbol{\tau})$, then a single convolution $\Psi^s * \mathbf{U}$ over all points satisfying (3.11) costs

$$(3.12) \quad C_{\text{naive}}(N, n, D) := (2n^{D+1} - 1)(N - n + 1)^{D+1}$$

floating point operations. If ψ is separable, then

$$D^{\alpha^s} \psi(\mathbf{Y}, \boldsymbol{\tau}) = \phi_1^{(\alpha_1^s)}(\mathbf{Y}_1) \otimes \cdots \otimes \phi_D^{(\alpha_D^s)}(\mathbf{Y}_D) \otimes \phi_{D+1}^{(\alpha_{D+1}^s)}(\boldsymbol{\tau}),$$

so that only the vectors

$$\phi_d^{(\alpha_d^s)}(\mathbf{Y}_d) \in \mathbb{R}^{2m_d+1}, \quad d \in [D] \quad \text{and} \quad \phi_{D+1}^{(\alpha_{D+1}^s)}(\boldsymbol{\tau}) \in \mathbb{R}^{2m_{D+1}+1},$$

need to be computed for each $0 \leq s \leq S$. In this way the multi-dimensional arrays $(\Psi^s)_{s=0, \dots, S}$ are never directly constructed and convolutions can be carried out sequentially in each coordinate, which reduces the cost of computing $\Psi^s * \mathbf{U}$ dramatically to

$$(3.13) \quad C_{\text{sep}}(N, n, D) := (2n - 1)N^{D+1} \sum_{d=1}^{D+1} \left(1 - \frac{(n-1)}{N}\right)^d.$$

This technique of exploiting separability in high-dimensional computations is not new (see [22] for an early introduction) and is frequently utilized in scientific computing (see [3, 11] for examples in computational chemistry). The computational savings in general vary with n/N (see Figure 3.1 for plots of $C_{\text{naive}}/C_{\text{sep}}$ for a range of N and D values), but they are considerable for all routines involved in WSINDy_PDE. For example, with $n = N/2$, we have $C_{\text{naive}} = \mathcal{O}(N^{2D+2})$ while $C_{\text{sep}} = \mathcal{O}(N^{D+2})$, hence exploiting separability reduces the complexity by a factor of N^D .

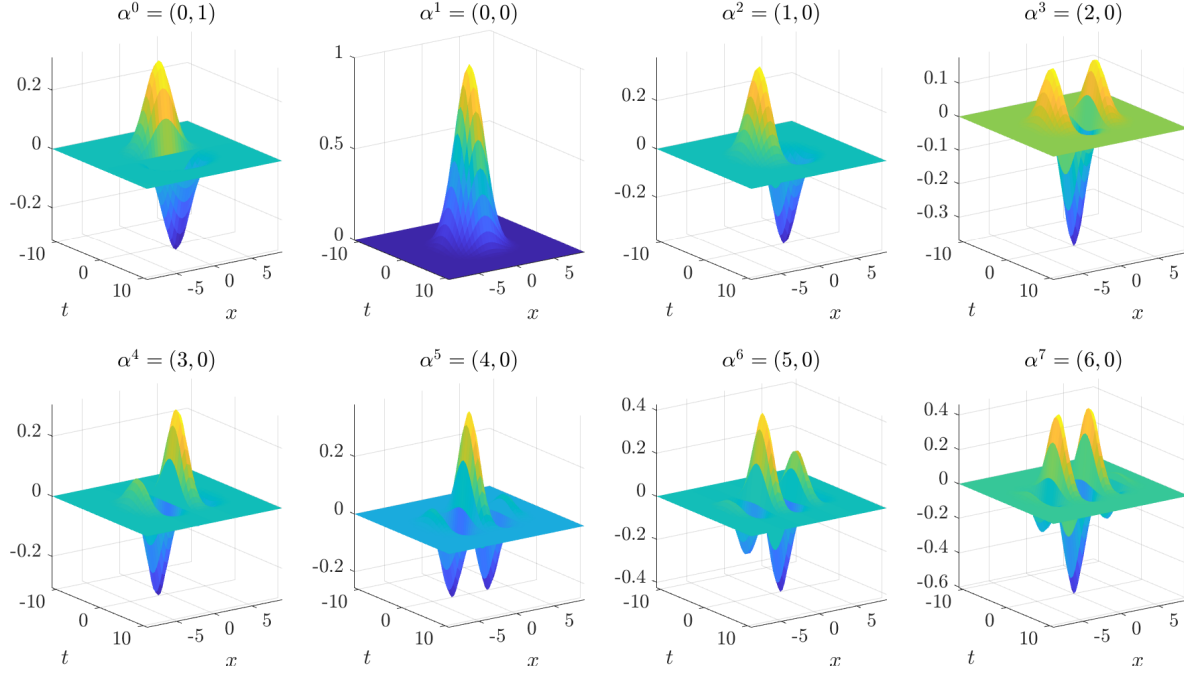


FIG. 3.2. Plots of reference test function ψ and partial derivatives $D^{\alpha^s} \psi$ used for identification of the Kuramoto-Sivashinsky equation (4.3). The upper left plot shows ψ_t , the bottom right shows $(\partial^6/\partial x^6)\psi$. See Section 4.1 and Table 2 for more details.

3.3. Piecewise-Polynomial Reference Test Functions. As demonstrated above, computation of \mathbf{G} and \mathbf{b} as in (3.6) using a separable reference test function ψ requires only that we select appropriate 1D coordinate test functions $(\phi_d)_{d \in [D+1]}$. WSINDy_PDE involves choosing coordinate test functions from the space \mathcal{S} of unimodal piecewise polynomials of the form

$$(3.14) \quad \phi(x) = \begin{cases} C(x-a)^p(b-x)^q & a < x < b, \\ 0 & \text{otherwise,} \end{cases}$$

where $p, q \geq 1$ and the normalization

$$C = \frac{1}{p^p q^q} \left(\frac{p+q}{b-a} \right)^{p+q}$$

ensures that $\|\phi\|_\infty = 1$. Functions $\phi \in \mathcal{S}$ are non-negative, unimodal, compactly-supported in $[a, b]$, and have $\lfloor \min\{p, q\} \rfloor - 1$ continuous derivatives. Larger p and q imply faster decay towards the endpoints (a, b) and for $p = q$ we refer to p as the degree of ϕ . As demonstrated in [20], if the trapezoidal rule is used to numerically integrate by parts a smooth function f against $\phi \in \mathcal{S}$, the integration error can be made arbitrarily small by choosing higher degree p without refining the grid. See Figure 3.2 for a visualization of ψ constructed from tensor products of functions from \mathcal{S} , along with partial derivatives $D^{\alpha^s} \psi$ for a range of α^s values.

To assemble the reference test function ψ from one-dimensional test functions $(\phi_d)_{d \in [D+1]} \subset \mathcal{S}$ along each coordinate, we must determine the parameters (a_d, b_d, p_d, q_d) in the formula (3.14) for each ϕ_d . We explain this process for $d \in [D]$, the values along the time axis ($d = D + 1$) are obtained identically by

replacing \mathbf{Y}_d with τ . By defining the reference grid $(\mathbf{Y}, \boldsymbol{\tau})$ to be centered at zero, each ϕ_d is centered at zero and so setting $[a_d, b_d] = [-b_d, b_d]$ for some endpoint value $b_d > 0$ reduces the parameter set to (b_d, p_d, q_d) .

In addition, to simplify the method, we use $p_d = q_d$ so that each ϕ_d is symmetric. Once p_d is specified, the vectors $(\phi_d^{(\alpha_d^s)}(\mathbf{Y}_d))_{0 \leq s \leq S}$ may easily be obtained from a function with support $[-1, 1]$ through scaling: we first compute the order- (α_d^s) derivatives $\tilde{\phi}_{p_d}^{(\alpha_d^s)}(\mathbf{n}_d)$ of the function

$$\tilde{\phi}_{p_d}(x) := \begin{cases} (1 - x^2)^{p_d}, & -1 < x < 1 \\ 0, & \text{otherwise} \end{cases}$$

on the scaled grid $\mathbf{n}_d := (n/m_d)_{-m_d \leq n \leq m_d} \subset [-1, 1]$, and then set

$$\phi_d^{(\alpha_d^s)}(\mathbf{Y}_d) = \frac{1}{b_d^{\alpha_d^s}} \tilde{\phi}_{p_d}^{(\alpha_d^s)}\left(\frac{\mathbf{Y}_d}{b_d}\right) = \frac{1}{(m_d \Delta x)^{\alpha_d^s}} \tilde{\phi}_{p_d}^{(\alpha_d^s)}(\mathbf{n}_d).$$

In this way, the number of parameters for specifying ψ is $2D + 2$ and includes the polynomial degrees $\mathbf{p} := (p_d)_{d \in [D+1]}$ and the support sizes $\mathbf{m} := (m_d)_{d \in [D+1]}$. To further reduce the number of parameters, we take the following approach: the user specifies the support sizes \mathbf{m} , which determine the supports $[-b_d, b_d]$ of ϕ_d by $b_d = m_d \Delta x$. The polynomial degrees \mathbf{p} are then computed by enforcing sufficient regularity and decay to the endpoints:

$$p_d = \min \left\{ p \geq \bar{\alpha}_d + 1 : \tilde{\phi}_p \left(1 - \frac{1}{m_d}\right) \leq 10^{-16} \right\},$$

where $\bar{\alpha}_d := \max_{0 \leq s \leq S} (\alpha_d^s)$. In this way, we ensure $\phi_d \in C^{\bar{\alpha}_d}(\mathbb{R})$ so that the test function ψ is smooth enough to integrate by parts as many times as necessary, and we enforce that ϕ_d decays quickly enough as $x \rightarrow \pm b_d$ so that the trapezoidal rule may be used with nearly negligible integration error (see [20]). Altogether, the steps for arriving at the test function coefficients $(\phi_d^{(\alpha_d^s)}(\mathbf{Y}_d))_{0 \leq s \leq S}$ are contained in Algorithm 3.1.

Algorithm 3.1 $(\phi_d^{(\alpha_d^s)}(\mathbf{Y}_d))_{0 \leq s \leq S} = \text{get_test_fcns}(N_d, \Delta x, \Delta t; \boldsymbol{\alpha}, m_d)$:

- 1: **if** $m_d > \frac{N_d - 1}{2}$ or $m_d \leq 1$ **then**
- 2: **return** (“ERROR: invalid support size m_d ”)
- 3: **BREAK**
- 4: **end if**
- 5: Set $\bar{\alpha}_d = \max_{0 \leq s \leq S} (\alpha_d^s)$
- 6: Solve $p_d = \min \left\{ p \geq \bar{\alpha}_d + 1 : \tilde{\phi}_p \left(1 - \frac{1}{m_d}\right) \leq 10^{-16} \right\}$
- 7: Initialize $\mathbf{A} = \mathbf{0} \in \mathbb{R}^{(S+1) \times (2m_d+1)}$
- 8: **for** $s = 0 : S$ **do**
- 9: Compute the order- (α_d^s) derivatives $\mathbf{A}_s = \tilde{\phi}_{p_d}^{(\alpha_d^s)}(\mathbf{n}_d)$
- 10: Set $\phi_d^{(\alpha_d^s)}(\mathbf{Y}_d) = \frac{1}{(m_d \Delta x)^{\alpha_d^s}} \mathbf{A}_s$
- 11: **end for**

For completion, we note that the vectors $\tilde{\phi}_{p_d}^{(\alpha_d^s)}(\mathbf{n}_d) \in \mathbb{R}^{2m_d+1}$ in Algorithm 3.1 can be computed recursively using the product rule for derivatives and the factorization

$$\tilde{\phi}_{p_d}(x) = (1 - x)^{p_d} (1 + x)^{p_d} := \phi_-(x) \phi_+(x).$$

We recursively compute the $(2m_d + 1)(\bar{\alpha}_d + 1)$ values

$$\phi_{\pm}^{(\ell)}(n/m_d) = p_d(p_d - 1) \dots (p_d - \ell + 1)(1 \pm n/m_d)^{p_d - \ell}$$

for $n \in \{0, \dots, m_d\}$ and $\ell \in \{0, \dots, \bar{\alpha}_d\}$, which are then reused in the sums

$$\tilde{\phi}_{p_d}^{(\alpha_d^s)}(n/m_d) = \sum_{\ell=0}^{\alpha_d^s} \binom{\alpha_d^s}{\ell} \phi_{-}^{(\alpha_d^s - \ell)}(n/m_d) \phi_{+}^{(\ell)}(n/m_d).$$

Using the symmetry $\tilde{\phi}_{p_d}(-x) = \tilde{\phi}_{p_d}(x)$, the values for $-m_d \leq n \leq -1$ are then obtained by an appropriate sign change.

3.4. Query Points and Subsampling. Having computed the necessary values of the reference test function $\psi = \phi_1(x_1) \dots \phi_{D+1}(t)$ using Algorithm 3.1, the last step in constructing the Gram matrix \mathbf{G} and right-hand side \mathbf{b} is choosing the query points $\{(\mathbf{x}_k, t_k)\}_{k \in [K]} \subset (\mathbf{X}, \mathbf{t})$. As noted in Remark 3.1, (\mathbf{x}_k, t_k) must satisfy (3.11) to ensure that $\psi(\mathbf{x}_k - x, t_k - t)$ is compactly supported in $\Omega \times [0, T]$ for each $k \in [K]$.

Since ψ is unimodal with a peak at the origin, $\psi(\mathbf{x}_k - x, t_k - t)$ will be unimodal with peak at (\mathbf{x}_k, t_k) , hence the placement of $\{(\mathbf{x}_k, t_k)\}_{k \in [K]}$ determines which regions of the spacetime dynamics are accentuated in the algorithm. In WSINDy for ODEs ([20]), an adaptive algorithm was designed for placement of test functions near steep gradients along the trajectory. Improvements in this direction for WSINDy_PDE are a topic of active research, however, for now we adopt a simpler uniform grid strategy by uniformly subsampling $\{(\mathbf{x}_k, t_k)\}_{k \in [K]}$ from (\mathbf{X}, \mathbf{t}) using subsampling frequencies $\mathbf{s} = (s_1, \dots, s_{D+1})$ along each coordinate, specified by the user. That is, along each one-dimensional grid \mathbf{X}_d , $\lfloor \frac{N_d - 2m_d}{s_d} \rfloor$ points are selected with uniform spacing $s_d \Delta x$ for $d \in [D]$ and $s_{D+1} \Delta t$ for $d = D+1$. This results in a $(D+1)$ -dimensional coarse grid with dimensions $\lfloor \frac{N_1 - 2m_1}{s_1} \rfloor \times \dots \times \lfloor \frac{N_{D+1} - 2m_{D+1}}{s_{D+1}} \rfloor$, which determines the number of query points

$$(3.15) \quad K = \prod_{d=1}^{D+1} \left\lfloor \frac{N_d - 2m_d}{s_d} \right\rfloor.$$

Integration still occurs on the fine grid, but only K such integrations are performed.

3.5. Algorithm. Putting together the pieces, the WSINDy_PDE algorithm for discovering PDE models from data is given in Algorithm 3.2. In order to use WSINDy_PDE on a given dataset, the user must specify each of the hyperparameters in Table 1. We now briefly discuss strategies for choosing hyperparameters.

3.5.1. Model Library. The model library is determined by the nonlinear functions $(f_j)_{j \in [J]}$ and the partial derivatives $\boldsymbol{\alpha}$ and is crucial to the well-posedness of the recovery problem. If the library is too large, linear dependence between functions prevents selection of the correct model. In the case of PDEs, many models can be derived from the desired model and may be numerically equivalent, some even preferred by the sequential thresholding routine over others. For instance, the function $u(x, t) = \sin^2((x + ct)/4)$ solves both

$$(3.16) \quad u_t = c u_x \quad \text{and} \quad u_t = -8 c u_{xxx},$$

yet since $|-8c| > |c|$, sequential thresholding will prefer the second equation over the first, when the simple advection equation is clearly preferred. Selection of minimal yet powerful model libraries is therefore an important topic for future research.

Algorithm 3.2 $\hat{\mathbf{w}} = \text{WSINDy_PDE}(\mathbf{U}, (\mathbf{X}, \mathbf{t}); (f_j)_{j \in [J]}, \boldsymbol{\alpha}, \mathbf{m}, \mathbf{s}, \lambda, \gamma)$:

```

1: for  $d = 1 : D + 1$  do
2:   Compute  $(\phi_d^{(\alpha_s^s)}(\mathbf{Y}_d))_{0 \leq s \leq S} = \text{get\_test\_fcns}(N_d, \Delta x, \Delta t; \boldsymbol{\alpha}, m_d)$  using Algorithm 3.1
3: end for
4: Subsample query points  $\{(\mathbf{x}_k, t_k)\}_{k \in [K]} \subset (\mathbf{X}, \mathbf{t})$  using subsampling frequencies  $\mathbf{s} = (s_1, s_2, \dots, s_{D+1})$ ;
5: for  $k = 1 : K$  do
6:   Compute  $k$ th right-hand side entry  $\mathbf{b}_k = \Psi^0 * \mathbf{U}(\mathbf{x}_k, t_k)$ , utilizing separability;
7: end for
8: for  $j = 1 : J$  do
9:   Compute  $f_j(\mathbf{U})$ ;
10:  for  $s = 1 : S$  do
11:    for  $k = 1 : K$  do
12:      Compute Gram matrix entry  $\mathbf{G}_{k,(s-1)J+j} = \Psi^s * f_j(\mathbf{U})(\mathbf{x}_k, t_k)$ , utilizing separability;
13:    end for
14:  end for
15: end for
16: Solve the regularized least-squares problem using sequential thresholding with parameter  $\lambda$ :
```

$$\hat{\mathbf{w}} = \operatorname{argmin}_{\mathbf{w}} \left\{ \|\mathbf{G}\mathbf{w} - \mathbf{b}\|_2^2 + \gamma^2 \|\mathbf{w}\|_2^2 \right\}.$$

Hyperparameter	Domain	Description
$(f_j)_{j \in [J]}$	$C(\mathbb{R})$	trial function library
$\boldsymbol{\alpha} = (\alpha_s)_{s=0, \dots, S}$	$\mathbb{N}^{(S+1) \times (D+1)}$	partial derivative library
$\mathbf{m} = (m_d)_{d \in [D+1]}$	\mathbb{N}^{D+1}	support sizes for 1D test functions $(\phi_d)_{d \in [D+1]}$
$\mathbf{s} = (s_d)_{d \in [D+1]}$	\mathbb{N}^{D+1}	subsampling frequencies for query points $\{(\mathbf{x}_k, t_k)\}_{k \in [K]}$
λ	$(0, \infty)$	sparsity parameter, enforces $\min_{\hat{\mathbf{w}} \neq 0} \hat{\mathbf{w}} \geq \lambda$
γ	$(0, \infty)$	Tikhonoff regularization parameter

TABLE 1

Hyperparameters for the WSINDy-PDE algorithm 3.2. Note that the number of query points K is determined from \mathbf{m} and \mathbf{s} using (3.15).

Throughout the examples below we use polynomials and trigonometric functions for $(f_j)_{j \in [J]}$, particularly because these sets are dense in a wide variety of function spaces. One could easily include exponentials or rational functions, and since the weak form does not require direct numerical differentiation, one could also experiment with piecewise continuous functions. In this work we choose $\boldsymbol{\alpha}$ without any cross-terms (i.e. $\partial^2/\partial x \partial y$ is omitted), although this choice is clearly problem dependent.

3.5.2. Discretization. Having chosen a model library, weak discretization of the discovery problem (i.e. arrival at the linear system $\mathbf{b} = \mathbf{G}\mathbf{w}^*$) is fully determined by \mathbf{m} and \mathbf{s} . Larger m_d (i.e. larger support of

the one-dimensional test function ϕ_d) results in a lower polynomial degree p_d , which leads to \mathbf{G} with better conditioning since then $\left\| \phi_d^{(\alpha_d^s)} \right\|_\infty$ grows more slowly as α_d^s increases. On the other hand, if m_d is too large (i.e. on the order of $N_d/2$), then the test function ϕ_d under-resolves features in the d th coordinate. A balance must be struck between choosing m_d that is too small to avoid poor conditioning and too large to resolve the model. In the examples below, we heuristically choose \mathbf{m} to achieve this balance, except in the case of Navier-Stokes (see Section 4.5) where we resorted to a minimal parameter sweep over \mathbf{m} and \mathbf{s} values.

The subsampling frequencies \mathbf{s} are chosen to avoid construction of linear systems that are unnecessarily large. As demonstrated below, often only a sparse selection of query points $\{(\mathbf{x}_k, t_k)\}_{k \in [K]}$ is needed to recover the model, despite reasonably high model complexity and/or large datasets. Unlike for WSINDy for ODEs [20], we do not delve into adaptive placement of test functions or query points in this article, favoring the simplest implementation procedures to avoid overcomplicating the method. We leave a systematic study of the necessary number of regression points K and optimal placement of query points to future work.

3.5.3. Sparsity and Regularization. The parameter λ enforces sparsity by regressing onto coefficients that satisfy $|\hat{\mathbf{w}}_{sj}| \geq \lambda$. Such sequential thresholding measures may be replaced by other sparsification schemes if so desired. The regularization γ is particularly useful in preventing selection of two nearby terms that end up cancelling out in the resulting model (see Section 4.3 on the Sine-Gordon equation), however in most cases we set $\gamma = 0$. Both λ and γ are chosen with soft adherence to the true coefficients, and we leave optimization of these parameters to future work. As demonstrated in [26], it is possible to devise a learning algorithm to train these parameters, but this is not explored here.

Remark 3.2. In WSINDy for ODEs [20], an approximate covariance matrix Σ was derived from the test functions using the fact that the derivative ϕ' of the test function amplifies the noise in a predictable manner. This allowed for the generalized least-squares approach

$$\hat{\mathbf{w}} = \operatorname{argmin}_{\mathbf{w}} \left\{ (\mathbf{G}\mathbf{w} - \mathbf{b})^T \Sigma^{-1} (\mathbf{G}\mathbf{w} - \mathbf{b}) + \gamma^2 \|\mathbf{w}\|_2^2 \right\}.$$

In the current setting, the same argument does not apply, as the largest noise amplification occurs in columns of the Gram matrix \mathbf{G} (due to higher derivatives of ϕ_d), and predicting this effect *a priori* would require knowledge of the nonzero entries of the weight vector \mathbf{w}^* . We leave the derivation of a suitable approximate covariance matrix Σ for future work, and for now adopt the ordinary least squares approach ($\Sigma = \mathbf{I}$).

4. Examples. We now demonstrate the effectiveness of WSINDy-PDE on the five systems listed in Section 2, with each system increasing the computational complexity, whether by increasing the number of spatial dimensions or the number of state variables. Since the behavior of each PDE is significantly different from the rest, and the numerical solvers used vary from example to example, we present the results of each system separately. The overarching themes include robustness to noise, accurate recovery in both small-noise and large-noise regimes, the use of small datasets or sparse subsampling from large datasets, identification from large libraries with linear dependencies, and fast computation.

To test the robustness to noise, a synthetic “observed” dataset

$$\mathbf{U} = \mathbf{U}^* + \epsilon$$

is obtained from adding white noise ϵ with variance σ^2 to each point of the exact simulation data \mathbf{U}^* , where

$$\sigma = \sigma_{SNR} \|\mathbf{U}^*\|_{RMS} := \sigma_{SNR} \left(\frac{1}{(N_1 \cdots N_D N_{D+1})} \sum_{k_1=1}^{N_1} \cdots \sum_{k_{D+1}=1}^{N_{D+1}} (\mathbf{U}_{k_1, \dots, k_{D+1}}^*)^2 \right)^{1/2}$$

and σ_{SNR} is specified beforehand. We then compute the true signal-to-noise ratio σ_{SNR}^* between the multi-dimensional noise array ϵ and the exact data \mathbf{U}^* , which is defined by

$$(4.1) \quad \sigma_{SNR}^* := \frac{\|\epsilon\|_{RMS}}{\|\mathbf{U}^*\|_{RMS}}.$$

In each example below, σ_{SNR}^* matches the specified σ_{SNR} to four significant digits and so we only list σ_{SNR} . In the cases where the state variable itself is multi-component, as in the nonlinear Schrödinger equation (4.2), reaction-diffusion system (4.4), and Navier-Stokes (4.5), a separate variance σ^2 is used to compute the noise ϵ in each component, so that σ_{SNR} is the same in each component.

To assess the accuracy of the method, we list the recovered models along with the relative maximum error in the identified coefficients:

$$(4.2) \quad E(\hat{\mathbf{w}}) := \max_{s,j} \left(\frac{|\hat{\mathbf{w}}_{(s-1)J+j} - \mathbf{w}_{(s-1)J+j}^*|}{|\mathbf{w}_{(s-1)J+j}^*|} \right)$$

where $E(\hat{\mathbf{w}}) = \infty$ for recovered models with terms differing from those of the true model (see the bottom rows of Tables 3, 5, 7, 9 and 11). The error $E(\hat{\mathbf{w}})$ determines the number of significant digits listed in the coefficients. Specifically, for noisy data we record $-\lfloor \log_{10}(E(\hat{\mathbf{w}})) \rfloor$ digits past the decimal if the system is correctly identified, while for noise-free data the number of significant digits is often large and so only $E(\hat{\mathbf{w}})$ is listed.

Each experiment below was carried out on an 8-core Intel i7-2670QM CPU with 2.2 GHz and 8 GB of RAM. With the exception of the Navier-Stokes equations, which were simulated using the immersed boundary projection method in C++ [29], all computations were performed in MATLAB 2019b.

4.1. Kuramoto-Sivashinsky. The first system we examine is the Kuramoto-Sivashinsky (KS) equation,

$$(4.3) \quad u_t = -\frac{1}{2} (u^2)_x - u_{xx} - u_{xxxx},$$

which contains a single state variable u in one spatial dimension and time. A solution is obtained for $(x, t) \in [0, 32\pi] \times [0, 150]$ with periodic boundary conditions using ETDRK4 timestepping and Fourier-spectral differentiation [14] with $N_1 = 256$ points in space and $N_2 = 1500$ points in time. For system identification we used 301 equally-spaced points in time at resolution $\Delta t = 0.5$ from the full simulation and kept all points in space for a dataset \mathbf{U} with a 77,056 points total. Table 2 lists the input parameters for the WSINDy_PDE algorithm. In words, the nonlinear functions $(f_j)_{j \in [7]}$ are the monomials up to degree 6 and the partial derivatives $\boldsymbol{\alpha}$ include all derivatives in x up to order 6, resulting in a model library with 43 terms of the form $D^{\alpha^s}(u^j)$. The reference test function ψ is supported on $2m_1 + 1 = 47$ points in x and $2m_2 + 1 = 45$ points in the t , resulting in polynomial degrees are $\mathbf{p} = (p_1, p_2) = (15, 15)$ (see Section 3.3). The query points $\{(\mathbf{x}_k, t_k)\}_{k \in [660]}$ include every 11th point in x and every 8th point in t . These library

$(f_j(u))_{j \in [J]}$	α	\mathbf{m}	\mathbf{s}	λ	γ
$(u^{j-1})_{j \in [7]}$	$((\ell, 0))_{0 \leq \ell \leq 6}$	(23, 22)	(11, 8)	0.05	0

TABLE 2

Input parameters to WSINDy-PDE used to discover KS.

$100(\sigma_{SNR})\%$	Identified System	$E(\hat{\mathbf{w}})$
0%	$u_t = -0.5(u^2)_x - 1.0u_{xx} - 1.0u_{xxxx}$	1.9e-06
10%	$u_t = -0.499(u^2)_x - 0.995u_{xx} - 0.996u_{xxxx}$	5.0e-03
20%	$u_t = -0.49(u^2)_x - 0.98u_{xx} - 0.98u_{xxxx}$	2.1e-02
30%	$u_t = -0.49(u^2)_x - 0.99u_{xx} - 0.99u_{xxxx}$	1.1e-02
40%	$u_t = -0.48(u^2)_x - 0.96u_{xx} - 0.95u_{xxxx}$	9.7e-02
50%	$u_t = -0.48(u^2)_x - 0.96u_{xx} - 0.97u_{xxxx}$	4.1e-02
60%	$u_t = -0.47(u^2)_x - 0.96u_{xx} - 1.10u_{xxxx}$ $-0.069(u^2)_{xxx} - 0.16u_{xxxxxx}$	∞

TABLE 3

Identified systems from KS data with incorrect terms in red. WSINDy-PDE is capable of recovering the correct system up to signal-to-noise ratios as high as 50% ($\sigma_{SNR} = 0.5$, see equation (4.1)), while for 60% noise, all correct terms are identified along with two incorrect terms.

and discretization choices result in a Gram matrix \mathbf{G} with dimensions 660×43 . The average wall time for running the algorithm start to finish is 0.09 seconds.

Identified systems and respective noise levels for KS data are given in Table 3. As desired, for noise-free data (top row) the correct system is identified to high accuracy (the identified weights \mathbf{w}^* are correct to nearly six digits), due to the low integration error induced by the chosen test functions. We then observe the remarkable capacity for WSINDy-PDE to handle large amounts of noise, as the correct system is identified with modest coefficient error up until 60% white noise is added ($\sigma_{SNR} = 0.6$, see equation (4.1)), at which point the correct terms are identified along with two spurious nonlinear dispersion and hyper-diffusion terms. For comparison, the original SINDy approach begins to fail in the presence of only 1% noise, returning the correct model with $\mathcal{O}(1)$ errors in the coefficients [26]. See Figure 4.1 for a visual comparison of the 0% noise and 50% noise solutions, the latter identified correctly to nearly two significant digits.

Remark 4.1. The KS equation (4.3) is a regularization of the shock-forming inviscid Burgers equation

$$u_t = -\frac{1}{2}(u^2)_x.$$

Another regularization of inviscid Burgers is the Korteweg-De Vries (KdV) equation,

$$u_t = -\frac{1}{2}(u_x)^2 - u_{xxx}.$$

We also performed WSINDy-PDE on KdV, but do not report the results here as they are qualitatively similar to those of KS, including recovery of the correct terms with 2 digit accuracy in the weights from data with 50% noise.

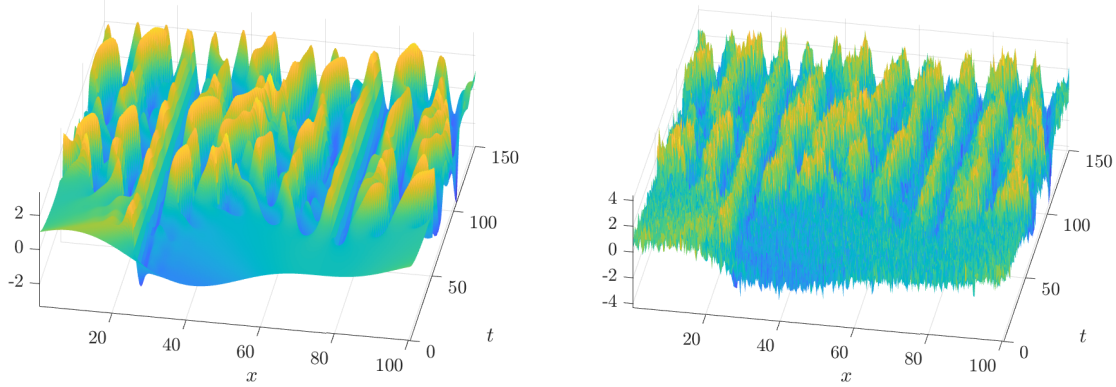


FIG. 4.1. *Kuramoto-Sivashinsky data*. *Left*: noise-free dataset. *Right*: dataset from row 6 of Table 3 with 50% noise ($\sigma_{SNR} = 0.5$).

$(f_j(v, w))_{j \in [J]}$	α	m	s	λ	γ
$(v^n w^m)_{0 \leq n+m \leq 6}$	$((\ell, 0))_{0 \leq \ell \leq 6}$	(23, 21)	(11, 8)	0.05	0

TABLE 4
Input parameters to WSINDy_PDE used to discover NLS.

4.2. Nonlinear Schrödinger.

$$(4.4) \quad u_t = -\frac{i}{2}u_{xx} + |u|^2u$$

For the nonlinear Schrödinger equation (NLS) we reuse the same dataset from [26], containing $N_1 = 512$ points in space and $N_2 = 502$ timepoints, although we coarsen the data by keeping every other point in space and time. For system identification, we break the data into real and imaginary parts ($u = v + iw$) to recover the system

$$(4.5) \quad \begin{cases} v_t = \frac{1}{2}w_{xx} + v^2w + w^3 \\ w_t = -\frac{1}{2}v_{xx} - v^3 - vw^2. \end{cases}$$

The total number of data points in the resulting dataset (\mathbf{U}, \mathbf{V}) over the two state variables (v, w) is 128,512. The input parameters listed in Table 4 include a nonlinear function library $(f_j)_{j \in [J]}$ of monomials up to a total degree of 6 in both v and w and spatial derivatives up to order 6. The weak discretization parameters \mathbf{m} and \mathbf{s} differ only slightly from those in Table 2 due to the difference in size between the KS and NLS datasets. The resulting Gram matrix \mathbf{G} has dimensions 540×190 , hence the total library of functions and partial derivatives has increased from 43 in the KS example to 190 due to the presence of two state variables. The resulting average wall time for WSINDy_PDE applied to NLS data was 0.41 seconds.

Similar to KS, Table 5 shows that the correct system (4.5) is identified to high accuracy from noise-free data and with respectable accuracy in the presence of large amounts of noise. With 30% noise ($\sigma_{SNR} = 0.3$, see equation (4.1)) an addition monomial term is selected which would have been set to zero if greater sparsity were enforced (i.e. $\lambda \geq 0.12$). See Figure 4.2 for a visual comparison of the 0% noise and 25% noise solutions.

$100(\sigma_{SNR}) \%$	Identified System	$E(\hat{\mathbf{w}})$
0	$\begin{cases} v_t = 0.5w_{xx} + 1.0v^2w + 1.0w^3 \\ w_t = -0.5v_{xx} - 1.0v^3 - 1.0vw^2 \end{cases}$	$3.8e-07$
10%	$\begin{cases} v_t = 0.498w_{xx} + 0.995v^2w + 0.998w^3 \\ w_t = -0.496v_{xx} - 0.997v^3 - 0.992vw^2 \end{cases}$	$8.0e-03$
20%	$\begin{cases} v_t = 0.48w_{xx} + 0.99v^2w + 0.97w^3 \\ w_t = -0.48v_{xx} - 0.99v^3 - 0.97vw^2 \end{cases}$	$4.1e-02$
25%	$\begin{cases} v_t = 0.47w_{xx} + 0.99v^2w + 0.97w^3 \\ w_t = -0.46v_{xx} - 0.97v^3 - 0.98vw^2 \end{cases}$	$8.0e-02$
30%	$\begin{cases} v_t = 0.46w_{xx} + 0.95v^2w + 0.97w^3 \\ w_t = -0.46v_{xx} - 1.00v^3 - 0.96vw^2 + 0.12v \end{cases}$	∞

TABLE 5

Identified systems from NLS data with incorrect terms in red. WSINDy_PDE is capable of recovering the correct system up to signal-to-noise ratios as high as 25% ($\sigma_{SNR} = 0.25$, see equation (4.1)), while for $\sigma_{SNR} = 0.3$, all correct terms are identified along with one incorrect terms.

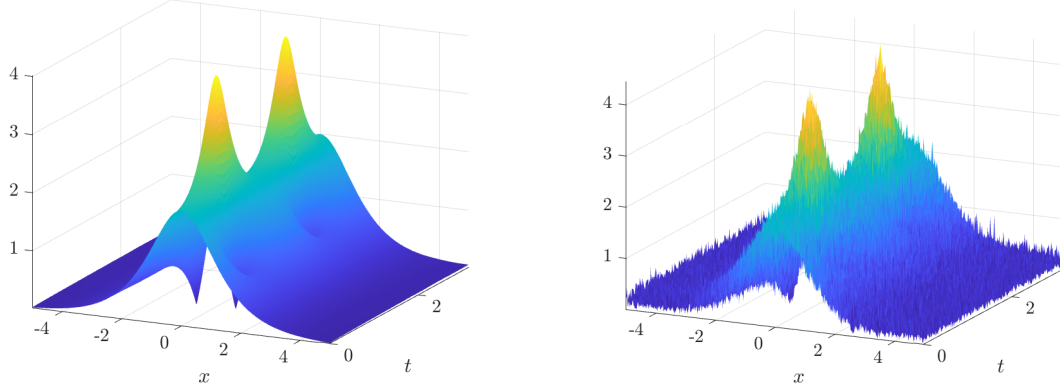


FIG. 4.2. Nonlinear Schrödinger amplitude data $\sqrt{u^2 + v^2}$. Left: noise-free dataset. Right: dataset with 25% noise from row 4 of Table 5.

4.3. Sine-Gordon. Our next example is the hyperbolic Sine-Gordon equation (SG) in two spatial dimensions and time:

$$(4.6) \quad u_{tt} = u_{xx} + u_{yy} - \sin(u).$$

SG demonstrates that WSINDy_PDE can easily be applied to hyperbolic problems as well as those with trigonometric nonlinearities, however the $\sin(u)$ term presents an interesting challenge in identifiability when combined with monomials. For larger noise, WSINDy_PDE occasionally selects terms from the Taylor expansion of $\sin(u)$, returning a splitting of the form

$$(4.7) \quad \tau \left(u - \frac{1}{6}u^3 + \dots \right) + (1 - \tau) \sin(u).$$

$(f_j(v, w))_{j \in [J]}$	α	\mathbf{m}	\mathbf{s}	λ	γ
$(u^{n-1})_{n \in [5]}, (\sin(mu), \cos(mu))_{m=1,2}$	$((\ell, 0, 0), (0, \ell, 0))_{0 \leq \ell \leq 4}$	$(26, 26, 12)$	$(5, 5, 3)$	0.05	0, 0.01

TABLE 6

Input parameters to WSINDy-PDE used to discover SG.

$100(\sigma_{SNR})\%$	Identified System	$E(\hat{\mathbf{w}})$
0%	$u_{tt} = 1.0u_{xx} + 1.0u_{yy} - 1.0 \sin(u)$	$3.7e-05$
5%	$u_{tt} = 1.000u_{xx} + 1.000u_{yy} - 1.002 \sin(u)$	$2.4e-03$
10%	$u_{tt} = 1.00u_{xx} + 1.00u_{yy} - 1.01 \sin(u)$	$1.2e-02$
15%	$u_{tt} = 1.00u_{xx} + 1.00u_{yy} - 1.03 \sin(u)$	$2.8e-02$
20%	$u_{tt} = 1.00u_{xx} + 1.00u_{yy} - 1.04 \sin(u)$	$3.8e-02$
25%	$u_{tt} = 1.00u_{xx} + 1.00u_{yy} - 1 \sin(u)$ $+4.32 \sin(u) - 0.31 \sin(2u) - 3.81u + 0.41u^3$ $+9.03 \cos(u) - 0.30 \cos(2u) - 8.73(1) + 3.96u^2 - 0.22u^4$	∞
25%*	$u_{tt} = 1.00u_{xx} + 1.00u_{yy} - 1.00 \sin(u) - 0.06u$	∞

TABLE 7

Identified systems from SG data with incorrect terms in red. WSINDy-PDE is capable of recovering the correct system up to a signal-to-noise ratio of 20% ($\sigma_{SNR} = 0.2$, see equation (4.1)), after which the method recovers terms from the Taylor expansion of sine and cosine resulting in an overall approximate cancellation. The bottom row (25%) is obtained by setting $\gamma = 0.01$, which greatly reduces the splitting over Taylor terms.*

This effect is altered by the Tikhonoff regularization parameter γ , which biases small weights. As γ is increased, fewer Taylor terms are identified along with $\sin(u)$.

A numerical solution is obtained using a pseudospectral method on the spatial domain $[-\pi, \pi] \times [-1, 1]$ with 64 equally-spaced points in x and 64 Legendre nodes in y . Periodic boundary conditions are enforced in x and homogeneous Dirichlet boundaries in y . Geometrically, waves can be thought of as propagating on a right cylinder with fixed ends. Leapfrog time-stepping is used to generate the solution until $T = 5$ with $\Delta t = 6e-5$. The solution is then interpolated onto a uniform grid in space with $N_1 = 403$ points in x and $N_2 = 129$ points in y . The dataset \mathbf{U} consists of $N_3 = 205$ equally-spaced points in time at a resolution of $\Delta t = 0.025$, subsampled from the total 83,000 timesteps, so that \mathbf{U} has a total of 10,657,335 datapoints.

Table 6 lists the parameters used to identify SG. The nonlinear function library consists of monomials up to degree 4 as well as $\sin(nu)$ and $\cos(nu)$ for $q = 1, 2$, and the partial derivatives include $\partial^s / \partial x^s$ and $\partial^s / \partial y^s$ for $s = 0, \dots, 4$. The resulting Gram matrix \mathbf{G} has 69,296 rows and 73 columns, in other words 69,296 query points and 73 candidate terms in the model library. The resulting average wall time for WSINDy-PDE applied to SG data was 23 seconds.

Table 7 shows that WSINDy-PDE is capable of discovering SG up to a noise level of 20% ($\sigma_{SNR} = 0.2$, see equation (4.1)). At 25% noise and regularization $\gamma = 0$, many false terms are identified from the Taylor

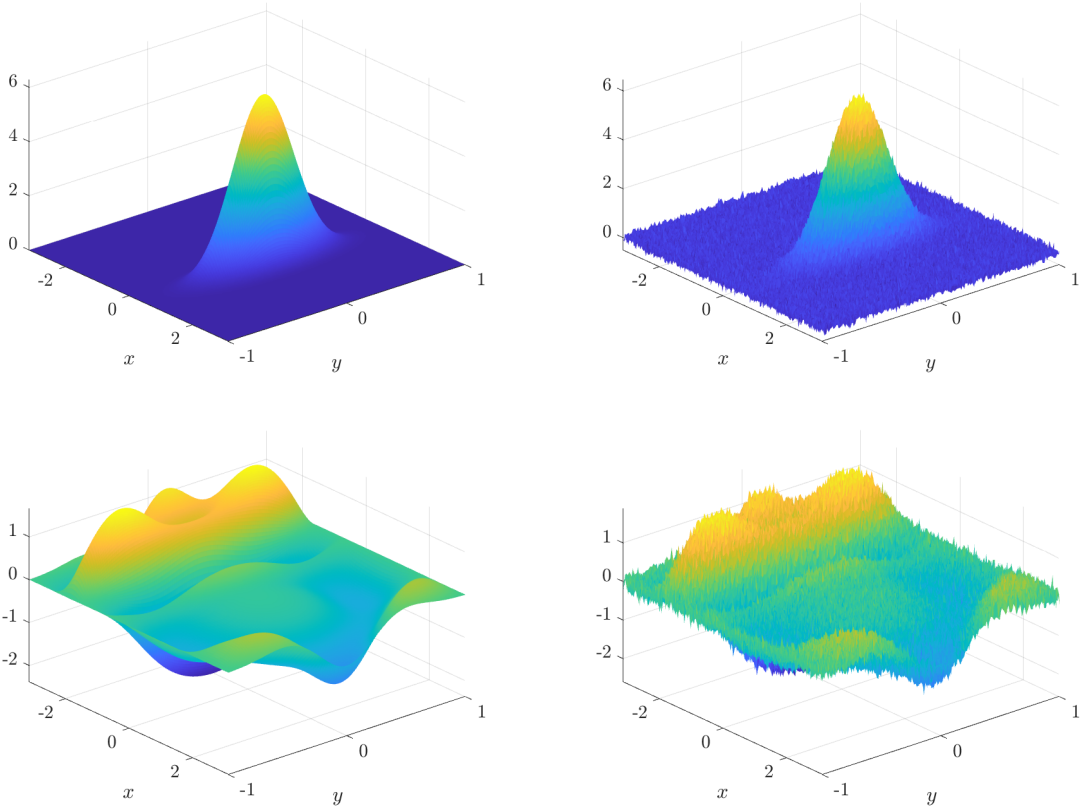


FIG. 4.3. Sine-Gordon data. Left: noise-free dataset. Right: dataset with 20% noise ($\sigma_{SNR} = 0.2$). The top row shows the initial conditions and the bottom row shows the final waveform.

expansions of sine and cosine. Specifically, looking more closely at the identified terms we see that

$$\begin{aligned} 4.32 \sin(u) - 0.31 \sin(2u) &= 3.70u - 0.31u^3 + \mathcal{O}(u^5), \\ 9.03 \cos(u) - 0.30 \cos(2u) &= 8.73 - 3.92u^2 + 0.18u^4 + \mathcal{O}(u^6) \end{aligned}$$

hence a splitting of the form (4.7) has been identified. With $\gamma = 0.01$, WSINDy_PDE identifies a more tractable system, with the only falsely identified term being $-0.06u$. In practice, from this one could easily identify that $\sin(u)$ is the dominant term in the PDE.

4.4. Reaction-Diffusion. We now increase the complexity of the problem by discovering the reaction-diffusion (RD) equation

$$(4.8) \quad \begin{cases} u_t = 0.1u_{xx} + 0.1u_{yy} + u - u^3 - uv^2 + u^2v + v^3 \\ v_t = 0.1v_{xx} + 0.1v_{yy} - u^3 - uv^2 + v - u^2v - v^3, \end{cases}$$

with data including two state variables (u, v) over two spatial dimensions and time. The main purpose of this example is for comparison with standard SINDy. The RD system above and numerical solution data is identical to that found in [26], where it was shown that the traditional SINDy approach was unable

$(f_j(v, w))_{j \in [J]}$	α	\mathbf{m}	\mathbf{s}	λ	γ
$(v^n w^m)_{0 \leq n+m \leq 4}$	$((\ell, 0, 0), (0, \ell, 0))_{0 \leq \ell \leq 5}$	$(30, 30, 22)$	$(3, 3, 12)$	0.05	0

TABLE 8

Input parameters to WSINDy_PDE used to discover RD.

$100(\sigma_{SNR})\%$	Identified System	$E(\hat{\mathbf{w}})$
0%	$\begin{cases} u_t = 0.1u_{xx} + 0.1u_{yy} + 1.0u - 1.0u^3 - 1.0uv^2 + 1.0u^2v + 1.0v^3 \\ v_t = 0.1v_{xx} + 0.1v_{yy} - 1.0u^3 - 1.0uv^2 + 1.0v - 1.0u^2v - 1.0v^3, \end{cases}$	$2.0e-06$
1%	$\begin{cases} u_t = 0.100u_{xx} + 0.100u_{yy} + 0.999u - 0.999u^3 - 0.999uv^2 + 1.000u^2v + 1.000v^3 \\ v_t = 0.100v_{xx} + 0.100v_{yy} - 1.000u^3 - 1.000uv^2 + 1.00v - 0.99u^2v - 0.99v^3, \end{cases}$	$9.6e-03$
5%	$\begin{cases} u_t = 0.099u_{xx} + 0.099u_{yy} + 1.00u - 0.99u^3 - 0.99uv^2 + 1.00u^2v + 1.00v^3 \\ v_t = 0.099v_{xx} + 0.099v_{yy} - 1.00u^3 - 0.99uv^2 + 1.000v - 1.000u^2v - 1.000v^3, \end{cases}$	$1.1e-03$
10%	$\begin{cases} u_t = 0.08u_{xx} + 0.08u_{yy} + 0.81u - 0.79u^3 - 0.79uv^2 + 0.79u^2v + 0.79v^3 + \textcolor{red}{0.18v} \\ v_t = 0.08v_{xx} + 0.08v_{yy} - 0.80u^3 - 0.80uv^2 + 0.80v - 0.79u^2v - 0.79v^3 - \textcolor{red}{0.17u} \end{cases}$	∞

TABLE 9

Identified systems from reaction-diffusion data with incorrect terms in red. WSINDy_PDE is capable of recovering the correct system up to a signal-to-noise ratio of 5% and with nearly 3 digits of accuracy in the weights. At 10% noise there are two falsely identified terms.

to identify the correct model for noise levels above 0.5%. WSINDy_PDE, on the other hand, is able to identify the correct system up to 5% noise, with 10% noise yielding a system that contains the correct terms in addition to an incorrect monomial term in each equation. The system that WSINDy_PDE identifies at 10% noise is also strikingly similar to the system that traditional SINDy identifies at 1% noise: the errors in weights associated with correct terms are of similar magnitude and the falsely identified terms are identical (see the supplemental material for [26]). This consistency is reassuring and suggests more systemic identifiability issues that can be studied and understood.

The system (4.8) is simulated over a doubly-periodic domain $(x, y) \in [-10, 10] \times [-10, 10]$ with $t \in [0, 10]$ using Fourier-spectral differentiation in space and method-of-lines time integration via MATLAB's `ode45` with default tolerance. The computational domain has dimensions $N_1 = N_2 = 256$ and $N_3 = 201$, hence the total number of data points over both state variable (\mathbf{U}, \mathbf{V}) is 26,345,472 data points. Input parameters for WSINDy_PDE applied to RD data are given in Table 8. The Gram matrix \mathbf{G} has dimensions $60,984 \times 156$ and the polynomial degrees used are $p_1 = p_2 = 14$ and $p_3 = 15$. Identified systems are listed in Table 9 and solutions snapshots are shown in Figure 4.4 for noise-free data and data with 10% noise. The resulting average wall time for WSINDy_PDE applied to RD data was 50 seconds.

4.5. Navier-Stokes. We close with the Navier-Stokes (NS) equations at Reynolds number $Re = 100$ in the classical setting of vortex shedding past a cylinder. The data $(\mathbf{U}, \mathbf{V}, \mathbf{W})$ consists of three state variables, the x and y components (u, v) of the two-dimensional flow velocity and the vorticity ω , over two spatial dimensions and time. Hence, the complexity has increased from the reaction-diffusion data by one state

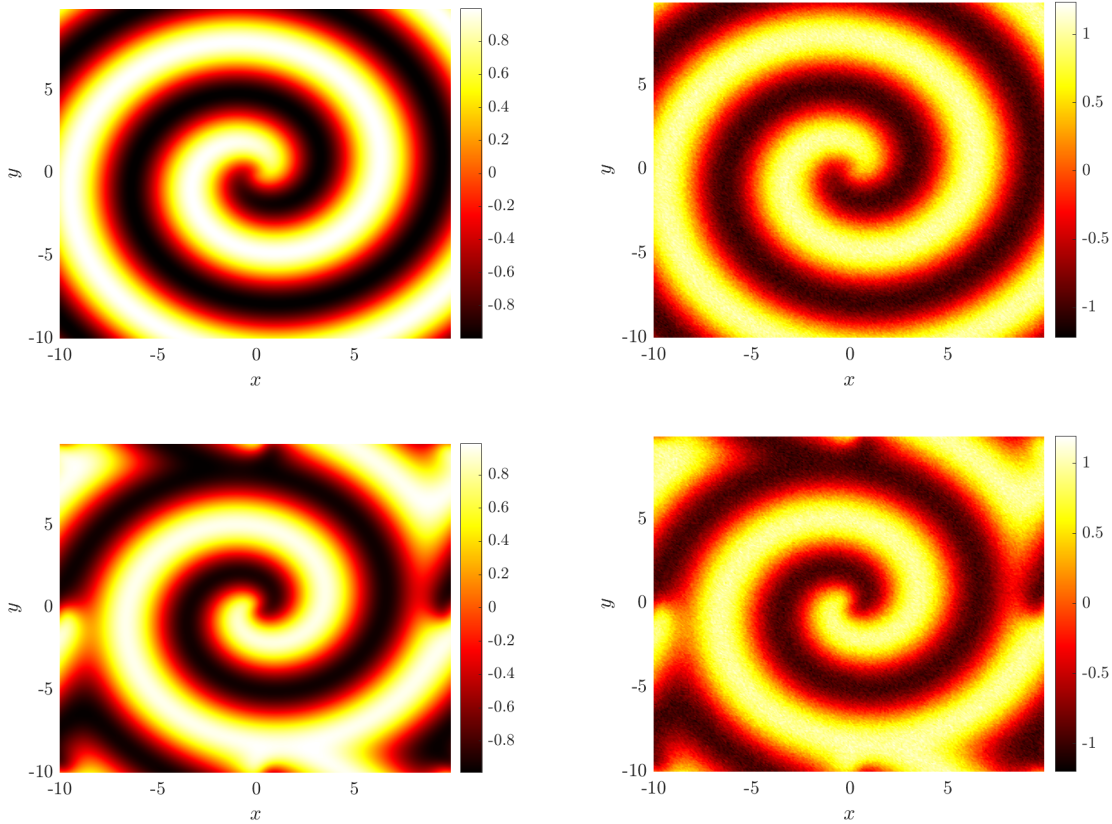


FIG. 4.4. Reaction-diffusion data. Left: noise-free dataset. Right: dataset with 10% noise ($\sigma_{SNR} = 0.1$). The top row shows u at time $t = 0$ and the bottom row shows u at time $t = 10$.

variable. We discover the conservation law for the vorticity ω in terms of (u, v) :

$$(4.9) \quad \omega_t = -(\omega u)_x - (\omega v)_y + 0.01\omega_{xx} + 0.01\omega_{yy}.$$

A solution is obtained on a spatial grid $(x, y) \subset [-1, 8] \times [-2, 2]$ with a ‘‘cylinder’’ of diameter 1 located at $(0, 0)$. The immersed boundary projection method [29] with 3rd-order Runge-Kutta timestepping is used to simulate the flow at spatial and temporal resolutions $\Delta x = \Delta t = 0.02$ for 2000 timesteps following the onset of the vortex shedding limit cycle. For the dataset $(\mathbf{U}, \mathbf{V}, \mathbf{W})$ we used points away from the cylinder and boundaries in the rectangle $(x, y) \in [1, 7.5] \times [-1.5, 1.5]$ at every tenth timestep, so that the dimensions of the computational grid are $324 \times 149 \times 201$ and the entire dataset consists of 29,110,428 data points.

To obtain the \mathbf{m} and \mathbf{s} parameters in Table 10, a parameter sweep was ran over 445 combinations resulting in a number of query points K between 5,000 and 10,000, for one instantiation of noise at each of the noise levels 2%, 4% and 6%. This was carried out on the University of Colorado Boulder Blanca Condo cluster ². The values $\mathbf{m} = (32, 32, 28)$ and $\mathbf{s} = (7, 7, 12)$ were chosen for their accuracy in recovered weights over the three instances of noise, however many parameter sets yielded similar recovery. The resulting Gram matrix \mathbf{G} has dimensions $6,422 \times 50$, hence only 6,422 query points in the computational domain were needed

²2X Intel Xeon 5218 at 2.3 GHz with 22 MB cache, 16 cores per cpu, and 384 GB ram.

$(f_j(v, w))_{j \in [J]}$	α	\mathbf{m}	\mathbf{s}	λ	γ
$\begin{cases} (\omega^n u^m v^q)_{0 \leq n+m+q \leq 2}, & \alpha^s = 0 \\ (\omega^n u^m v^q)_{0 \leq n+m+q \leq 3, n > 0}, & \alpha^s > 0 \end{cases}$	$((\ell, 0, 0), (0, \ell, 0))_{0 \leq \ell \leq 2}$	(32, 32, 28)	(7, 7, 12)	0.005	0

TABLE 10

Input parameters to WSINDy_PDE used to discover NS. For the model library, we exclude monomial source terms $\omega^n u^m v^q$ with total degree 3 and derivative terms $\partial^k / \partial x^k (\omega^n u^m v^q)$ and $\partial^k / \partial y^k (\omega^n u^m v^q)$ for which $n = 0$ to avoid linear dependencies.

$100(\sigma_{SNR})\%$	Identified System	$E(\hat{\mathbf{w}})$
0%	$\omega_t = -1.000(\omega u)_x - 0.999(\omega v)_y + 0.010\omega_{xx} + 0.0010\omega_{yy}$	5.7e-03
2%	$\omega_t = -1.000(\omega u)_x - 0.999(\omega v)_y + 0.010\omega_{xx} + 0.010\omega_{yy}$	5.9e-03
4%	$\omega_t = -1.000(\omega u)_x - 0.999(\omega v)_y + 0.010\omega_{xx} + 0.0010\omega_{yy}$	3.2e-03
6%	$\omega_t = -1.000(\omega u)_x - 0.999(\omega v)_y + 0.010\omega_{xx} + 0.010\omega_{yy}$	7.0e-03
8%	$\omega_t = -0.998(\omega u)_x - 0.996(\omega v)_y + 0.010\omega_{xx} + 0.010\omega_{yy}$ +0.008v - 0.008uv	NA
10%	$\omega_t = -0.996(\omega u)_x - 0.996(\omega v)_y + 0.010\omega_{xx} + 0.010\omega_{yy}$ +0.014v - 0.009uv	NA

TABLE 11

Navier-Stokes identified systems with incorrect terms in red.

to recover the dynamics. The resulting polynomial degrees for the reference test functions are $p_1 = p_2 = 13$ and $p_3 = 14$ and the resulting average wall time for computations is 13 seconds. Identified systems are listed in Table 11. Vorticity snapshots are shown in Figure 4.5 for noise-free data and data with 10% noise.

The main purpose of demonstrating WSINDy_PDE on Navier-Stokes data is to show that convective PDEs may be recovered in conservation form despite the divergence-free constraint used to simulate the flow. In [26] it is shown that the traditional SINDy approach is able to identify the vorticity equation in convective form

$$\omega_t = -u\omega_x - v\omega_y + 0.01\omega_{xx} + 0.01\omega_{yy}$$

from data with 1% noise, however the recovered system has large errors in the weights (e.g. a relative error of 17% in the coefficient of ω_{yy}), and the SVD is used to project onto dominant modes in an effort to denoise the data. The convective terms $u\omega_x$ and $v\omega_y$ do not directly fit into the form $D^{\alpha^s} g(u, v, \omega)$ necessary for applying WSINDy_PDE, and so the flux terms $\nabla \cdot (\omega \mathbf{u}^T) = (\omega u)_x + (\omega v)_y$ must be used. Nevertheless, as depicted in Table 11, WSINDy_PDE is able to recover equation (4.9) with much more accurate weights up to 6% noise, and without prior denoising. Furthermore, for higher noise levels, the falsely identified terms v and uv are explainable by the background flow of $U = 1$ in the x -direction. Using the values from row five of Table 11, we see that knowledge of the background flow gives the approximate cancellation

$$0.008v - 0.008uv = 0.008v(1 - u) \approx 0.008v(1 - U) = 0.$$

In addition, with higher sparsity λ these terms would not have been falsely identified.

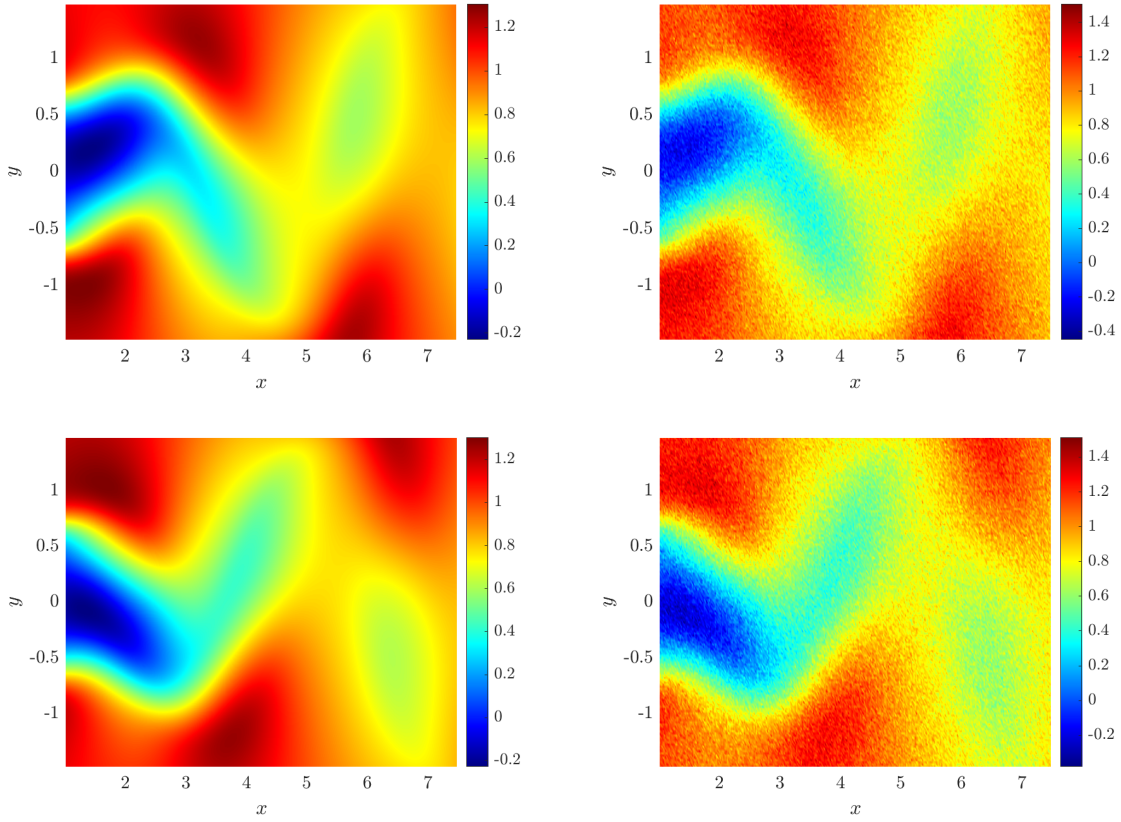


FIG. 4.5. Navier-Stokes vorticity data. Left: noise-free dataset. Right: dataset with 10% noise ($\sigma_{SNR} = 0.1$). Top and bottom rows show initial and final conditions.

5. Conclusion. The WSINDy_PDE algorithm opens the door to methods of data-driven model selection for spatiotemporal dynamics that do not require pointwise derivative approximations, black-box closure models (i.e. deep neural networks), dimensionality reduction or other noise filtering. The examples above suggest that WSINDy_PDE is more robust to noise than any existing algorithm for the discovery of PDEs ³. In addition, its computational efficiency suggest that WSINDy_PDE may be suitable for data-driven model selection in higher spatial dimensions and/or with higher-dimensional state variables.

As demonstrated in the Sine-Gordon and Navier-Stokes sections above (Section 4.3, Section 4.5) identifiability of certain models terms remains an issue in application of WSINDy_PDE, as with any model selection algorithm. For Sine-Gordon, this problem manifests in the form of selecting the correct term $\sin(u)$ in the presence of approximating terms from the monomial basis. For Navier-Stokes, the model library in Table 10 must be trimmed due to linear dependencies that result from the divergence-free constraint and the vorticity. Specifically, since

$$u_x + v_y = 0 \quad \text{and} \quad \omega = v_x - u_y,$$

³To the best of the authors' knowledge, recovery of PDEs with noise levels as high as 50% ($\sigma_{SNR} = 0.5$, defined in (4.1)) for $D = 1$ spatial dimension and time or 20% noise for $D = 2$ spatial dimensions (see Sections 4.1, 4.3) has not been previously reported in the literature.

nontrivial identities such as

$$\omega u + \omega v = (uv)_x - (uv)_y - \frac{1}{2}(u^2)_x - \frac{1}{2}(u^2)_y + \frac{1}{2}(v^2)_x + \frac{1}{2}(v^2)_y$$

arise which obscure identification of the desired vorticity equation, unless derivative terms which do not contain ω are removed from the library. Discerning that a given collection of differential operators is truly approximating a single operator that is either absent from the model library or has a small coefficient in the true PDE, for instance, is an ongoing problem in itself [42] and requires a certain level of expertise in the scientific area in question to solve.

Compared to other methods, WSINDy_PDE requires models to be posed in the “generalized conservative form” (2.1), which we repeat here for convenience:

$$D^{\alpha^0} u := D^{\alpha^1} g_1(u) + D^{\alpha^2} g_2(u) + \cdots + D^{\alpha^S} g_S(u) \quad x \in \Omega, t \in (0, T).$$

This should not be viewed as a limitation. Certainly, some stand-alone terms such as $(u_x)^2$ cannot be written as $D^\alpha g(u)$ for some function g and multi-index α . In the sequel we will explore model selection for such models. There are many ways to efficiently generalize WSINDy_PDE to ever-more challenging cases by leveraging the smoothness of test functions and the linearity of integration. As well as having analytical appeal and convenience, one may argue that the weak form of the dynamics is a more physically realistical and generalizable framework for describing the dynamics. By gathering information only on the system’s response to probes and measurements (i.e. integration against test functions), computations mirror the experimentalist.

In this article we have demonstrated that despite the challenges, integrating spacetime datasets against test functions is a feasible basis for model discovery, provided that careful choices are made about the test functions involved and the integration schemes. WSINDy_PDE is still very much in its infancy, with plenty of potential for optimization, extension, and even hybrid use with existing approaches that rely on neural networks, dimensionality reduction or other denoising.

6. Acknowledgements. This research was supported in part by the NSF/NIH Joint DMS/NIGMS Mathematical Biology Initiative grant R01GM126559 and in part by the NSF Computing and Communications Foundations Division grant CCF-1815983. This work also utilized resources from the University of Colorado Boulder Research Computing Group, which is supported by the National Science Foundation (awards ACI-1532235 and ACI-1532236), the University of Colorado Boulder, and Colorado State University. Code used in this manuscript is publicly available on GitHub at https://github.com/dm973/WSINDy_PDE.

REFERENCES

- [1] H. AKAIKE, *A new look at the statistical model identification*, IEEE Transactions on Automatic Control, 19 (1974), pp. 716–723, <https://doi.org/10.1109/TAC.1974.1100705>.
- [2] H. AKAIKE, *On entropy maximization principle*, in Applications of Statistics, P. R. Krishnaiah, ed., North Holland, Amsterdam, Netherlands, 1977, pp. 27–41.
- [3] G. BEYLKIN AND M. J. MOHLENKAMP, *Algorithms for numerical analysis in high dimensions*, SIAM Journal on Scientific Computing, 26 (2005), pp. 2133–2159.
- [4] D. M. BORTZ AND P. W. NELSON, *Model Selection and Mixed-Effects Modeling of HIV Infection Dynamics*, Bulletin of Mathematical Biology, 68 (2006), pp. 2005–2025, <https://doi.org/10.1007/s11538-006-9084-x>.
- [5] S. L. BRUNTON, J. L. PROCTOR, AND J. N. KUTZ, *Discovering governing equations from data by sparse identification of nonlinear dynamical systems*, Proceedings of the national academy of sciences, 113 (2016), pp. 3932–3937.
- [6] X. CHEN, J. DUAN, AND G. E. KARNIADAKIS, *Learning and meta-learning of stochastic advection-diffusion-reaction systems from sparse measurements*, arXiv preprint arXiv:1910.09098, (2019).
- [7] A. CORTIELLA, K.-C. PARK, AND A. DOOSTAN, *Sparse identification of nonlinear dynamical systems via reweighted ℓ_1 -regularized least squares*, arXiv preprint arXiv:2005.13232, (2020).
- [8] J. P. CRUTCHFIELD AND B. S. McNAMARA, *Equations of motion from a data series*, Complex systems, 1 (1987), p. 121.
- [9] M. DAI, T. GAO, Y. LU, Y. ZHENG, AND J. DUAN, *Detecting the maximum likelihood transition path from data of stochastic dynamic systems*, arXiv preprint arXiv:2004.11513, (2020).
- [10] B. M. DE SILVA, K. CHAMPION, M. QUADE, J.-C. LOISEAU, J. N. KUTZ, AND S. L. BRUNTON, *Pysindy: A python package for the sparse identification of nonlinear dynamics from data*, arXiv, (2020), pp. arXiv–2004.
- [11] R. J. HARRISON, G. BEYLKIN, F. A. BISCHOFF, J. A. CALVIN, G. I. FANN, J. FOSSE-TANDE, D. GALINDO, J. R. HAMMOND, R. HARTMAN-BAKER, J. C. HILL, ET AL., *Madness: A multiresolution, adaptive numerical environment for scientific simulation*, SIAM Journal on Scientific Computing, 38 (2016), pp. S123–S142.
- [12] M. HOFFMANN, C. FRÖHNER, AND F. NOÉ, *Reactive sindy: Discovering governing reactions from concentration data*, The Journal of Chemical Physics, 150 (2019), p. 025101.
- [13] S. H. KANG, W. LIAO, AND Y. LIU, *Ident: Identifying differential equations with numerical time evolution*, arXiv preprint arXiv:1904.03538, (2019).
- [14] A.-K. KASSAM AND L. N. TREFETHEN, *Fourth-order time-stepping for stiff pdes*, SIAM Journal on Scientific Computing, 26 (2005), pp. 1214–1233.
- [15] R. KELLER AND Q. DU, *Discovery of dynamics using linear multistep methods*, arXiv preprint arXiv:1912.12728, (2019).
- [16] J. H. LAGERGREN, J. T. NARDINI, R. E. BAKER, M. J. SIMPSON, AND K. B. FLORES, *Biologically-informed neural networks guide mechanistic modeling from sparse experimental data*, arXiv preprint arXiv:2005.13073, (2020).
- [17] J. H. LAGERGREN, J. T. NARDINI, G. MICHAEL LAVIGNE, E. M. RUTTER, AND K. B. FLORES, *Learning partial differential equations for biological transport models from noisy spatio-temporal data*, Proc. R. Soc. A., 476 (2020), p. 20190800, <https://doi.org/10.1098/rspa.2019.0800>.
- [18] G. LILLACCI AND M. KHAMMASH, *Parameter Estimation and Model Selection in Computational Biology*, PLoS Comput Biol, 6 (2010), p. e1000696, <https://doi.org/10.1371/journal.pcbi.1000696>.
- [19] N. M. MANGAN, J. N. KUTZ, S. L. BRUNTON, AND J. L. PROCTOR, *Model selection for dynamical systems via sparse regression and information criteria*, Proceedings of the Royal Society A: Mathematical, Physical and Engineering Sciences, 473 (2017), p. 20170009.
- [20] D. A. MESSENGER AND D. M. BORTZ, *Weak sindy: Galerkin-based data-driven model selection*, arXiv preprint arXiv:2005.04339, (2020).
- [21] J. T. NARDINI, J. H. LAGERGREN, A. HAWKINS-DAARUD, L. CURTIN, B. MORRIS, E. M. RUTTER, K. R. SWANSON, AND K. B. FLORES, *Learning equations from biological data with limited time samples*, arXiv preprint arXiv:2005.09622, (2020).
- [22] V. PEREYRA AND G. SCHERER, *Efficient computer manipulation of tensor products with applications to multidimensional approximation*, Mathematics of Computation, 27 (1973), pp. 595–605.
- [23] T. QIN, Z. CHEN, J. JAKEMAN, AND D. XIU, *Data-driven learning of non-autonomous systems*, arXiv preprint

arXiv:2006.02392, (2020).

[24] T. QIN, K. WU, AND D. XIU, *Data driven governing equations approximation using deep neural networks*, Journal of Computational Physics, 395 (2019), pp. 620–635.

[25] M. RAISSI, P. PERDIKARIS, AND G. E. KARNIADAKIS, *Machine learning of linear differential equations using Gaussian processes*, Journal of Computational Physics, 348 (2017), pp. 683–693.

[26] S. H. RUDY, S. L. BRUNTON, J. L. PROCTOR, AND J. N. KUTZ, *Data-driven discovery of partial differential equations*, Science Advances, 3 (2017), p. e1602614.

[27] S. H. RUDY, J. N. KUTZ, AND S. L. BRUNTON, *Deep learning of dynamics and signal-noise decomposition with time-stepping constraints*, Journal of Computational Physics, 396 (2019), pp. 483–506.

[28] H. SCHAEFFER AND S. G. MCCALLA, *Sparse model selection via integral terms*, Physical Review E, 96 (2017), p. 023302.

[29] K. TAIRA AND T. COLONIUS, *The immersed boundary method: A projection approach*, J. Comput. Phys., 225 (2007), pp. 2118–2137.

[30] S. THALER, L. PAEHLER, AND N. A. ADAMS, *Sparse identification of truncation errors*, Journal of Computational Physics, 397 (2019), p. 108851.

[31] T. TONI, D. WELCH, N. STRELKOWA, A. IPSEN, AND M. P. STUMPF, *Approximate Bayesian computation scheme for parameter inference and model selection in dynamical systems*, J. R. Soc. Interface., 6 (2009), pp. 187–202, <https://doi.org/10.1098/rsif.2008.0172>.

[32] G. TRAN AND R. WARD, *Exact recovery of chaotic systems from highly corrupted data*, Multiscale Modeling & Simulation, 15 (2017), pp. 1108–1129.

[33] W.-X. WANG, R. YANG, Y.-C. LAI, V. KOVANIS, AND C. GREBOGI, *Predicting catastrophes in nonlinear dynamical systems by compressive sensing*, Physical review letters, 106 (2011), p. 154101.

[34] Y. WANG, S. W. CHEUNG, E. T. CHUNG, Y. EFENDIEV, AND M. WANG, *Deep multiscale model learning*, Journal of Computational Physics, 406 (2020), p. 109071.

[35] Z. WANG, X. HUAN, AND K. GARIKIPATI, *Variational system identification of the partial differential equations governing the physics of pattern-formation: inference under varying fidelity and noise*, Computer Methods in Applied Mechanics and Engineering, 356 (2019), pp. 44–74.

[36] Z. WANG, X. HUAN, AND K. GARIKIPATI, *Identification of the partial differential equations governing microstructure evolution in materials: Inference over incomplete, sparse and spatially non-overlapping data*, arXiv preprint arXiv:2001.04816, (2020).

[37] Z. WANG, B. WU, K. GARIKIPATI, AND X. HUAN, *A perspective on regression and bayesian approaches for system identification of pattern formation dynamics*, arXiv preprint arXiv:2001.05646, (2020).

[38] D. J. WARNE, R. E. BAKER, AND M. J. SIMPSON, *Using Experimental Data and Information Criteria to Guide Model Selection for Reaction–Diffusion Problems in Mathematical Biology*, Bull Math Biol, 81 (2019), pp. 1760–1804, <https://doi.org/10.1007/s11538-019-00589-x>.

[39] H. WU AND L. WU, *Identification of significant host factors for HIV dynamics modelled by non-linear mixed-effects models*, Statist. Med., 21 (2002), pp. 753–771, <https://doi.org/10.1002/sim.1015>.

[40] K. WU AND D. XIU, *Numerical aspects for approximating governing equations using data*, Journal of Computational Physics, 384 (2019), pp. 200–221.

[41] K. WU AND D. XIU, *Data-driven deep learning of partial differential equations in modal space*, Journal of Computational Physics, 408 (2020), p. 109307.

[42] H. XU, H. CHANG, AND D. ZHANG, *Dlga-pde: Discovery of pdes with incomplete candidate library via combination of deep learning and genetic algorithm*, Journal of Computational Physics, (2020), p. 109584.

[43] L. ZHANG AND H. SCHAEFFER, *On the convergence of the SINDy algorithm*, Multiscale Modeling & Simulation, 17 (2019), pp. 948–972.

[44] S. ZHANG AND G. LIN, *Robust data-driven discovery of governing physical laws with error bars*, Proceedings of the Royal Society A: Mathematical, Physical and Engineering Sciences, 474 (2018), p. 20180305.

[45] S. ZHANG AND G. LIN, *Robust subsampling-based sparse Bayesian inference to tackle four challenges (large noise, outliers, data integration, and extrapolation) in the discovery of physical laws from*, arXiv preprint arXiv:1907.07788, (2019).